ANDERSSON ALIRIO ACEVEDO SERRATO

GEOCRONOLOGIA E EVOLUÇÃO DO SISTEMA HIDROTERMAL DO DEPÓSITO AURÍFERO DE JURUENA, PROVINCIA AURÍFERA DE ALTA FLORESTA (MT), BRASIL.

CAMPINAS

2014

NÙMERO: 477/2014
UNIVERSIDADE ESTADUAL DE CAMPINAS
INSTITUTO DE GEOCIENCIAS

ANDERSSON ALIRIO ACEVEDO SERRATO

"GEOCRONOLOGIA E EVOLUÇÃO DO SISTEMA HIDROTERMAL DO DEPÓSITO AURÍFERO DE JURUENA, PROVINCIA AURÍFERA DE ALTA FLORESTA (MT), BRASIL"

ORIENTADOR: PROF. DR. ROBERTO PEREZ XAVIER

DISSERTAÇÃO DE MESTRADO APRESENTADA AO INSTITUTO DE GEOCIÊNCIAS DA UNICAMP PARA OBTENÇÃO DO TÍTULO DE MESTRE EM GEOCIÊNCIAS NA ÁREA DE GEOLOGIA E RECURSOS NATURAIS

ESTE EXEMPLAR CORRESPONDE À VERSÃO FINAL DA DISSERTAÇÃO DEFENDIDA PELO ALUNO ANDERSSON ALIRIO ACEVEO SERRATO E ORIENTADO PELO PROF. DR. ROBERTO PEREZ XAVIER

CAMPINAS

2014

Ficha catalográfica
Universidade Estadual de Campinas
Biblioteca do Instituto de Geociências
Cássia Raquel da Silva - CRB 8/5752

Ac37g

Acevedo Serrato, Andersson Alirio, 1986-
Geornologia e evolução do sistema hidrotermal do depósito aurífero de Juruena, Província Aurífera de Alta Floresta (MT), Brasil / Andersson Alirio Acevedo Serrato. – Campinas, SP : [s.n.], 2014.

Orientador: Roberto Perez Xavier.
Dissertação (mestrado) – Universidade Estadual de Campinas, Instituto de Geociências.

1. Ouro - Minas e mineração - Alta Floresta (MT). 2. Mineralizações auríferas. 3. Metalogenia. 4. Geocronologia. 5. Isotópos estáveis. I. Xavier, Roberto Perez,1958-. II. Universidade Estadual de Campinas. Instituto de Geociências. III. Título.

Informações para Biblioteca Digital

Título em outro idioma: The evolution of the Paleoproterozoic Juruena intrusion-hosted gold deposit, northwestern sector of the Alta Floresta Gold Province (Mt), Brazil
Palavras-chave em inglês:
Gold - Mines and mineralization - Alta Floresta (MT)
Gold Mineralization
Metallogeny
Gechronology
Stable Isotopes
Área de concentração: Geologia e Recursos Naturais
Titulação: Mestre em Geociências
Banca examinadora:
Roberto Perez Xavier [Orientador]
Maria José Mesquita
Marcia Abrahão Moura
Data de defesa: 12-03-2014
Programa de Pós-Graduação: Geociências

UNICAMP

UNIVERSIDADE ESTADUAL DE CAMPINAS
INSTITUTO DE GEOCIÊNCIAS
PÓS-GRADUAÇÃO EM GEOCIÊNCIAS NA
ÀREA DE GEOLOGIA E RECURSOS NATURAIS

AUTOR: Andersson Alirio Acevedo Serrato

Geocronologia e evolução do sistema hidrotermal do depósito aurífero de Juruena, Província Aurífera de Alta Floresta (MT), Brasil

ORIENTADOR: Prof. Dr. Roberto Perez Xavier

Aprovado em: 12 / 03 / 2014

EXAMINADORES:

Prof. Dr. Roberto Perez Xavier _____ - Presidente

Profa. Dra. Maria José Maluf de Mesquita _____

Profa. Dra. Márcia Abrahão Moura _____

Campinas, 12 de março de 2014

Dedico este trabalho a toda minha família pela força,
apoio e paciência durante este período em que fiquei longe
de casa, à Juanita incondicional companheira
com quem compartilhei esta grande experiência

AGRADECIMENTO

Agradeço primeiramente a Deus, pela grande oportunidade que me deu de viver esta inolvidável experiência.

Ao meu orientador, Prof. Dr. Roberto Perez Xavier, primeiramente pela oportunidade que me foi dada, pela confiança, paciência e incentivo durante o desenvolvimento deste trabalho.

À pesquisadora, amiga e co-autora do artigo, Erin Marsh, pelos conselhos, apoio e confiança durante esta etapa da minha vida. Sem o seu apoio este trabalho teria sido ainda mais difícil.

Ao Prof. Dr. Richard Goldfarb agradeço por compartilhar sua experiência comigo, além de acreditar e dar completo apoio e motivação ao meu trabalho.

Ao "*United States Geological Survey- USGS"* pela oportunidade de desenvolver uma boa parte das analises nos seus laboratórios.

Ao CNPq pela concessão da minha bolsa de mestrado.

À "*Society of Economic Geologist* – SEG", pela bolsa concedida que sem dúvida foi um grande incentivo durante meu período de mestrado.

Ao capitulo estudantil da SEG que foi um apoio constante nesta minha tarefa de entender um pouco mais os depósitos minerais.

À Val, Gorete, Valdir e Rafael, que sempre tiveram boa disposição e fizeram nossa estadia mais simples.

Aos professores e amigos do IG que sempre estiveram presentes para me aconselhar nas diferentes etapas, durante o desenvolvimento da pesquisa.

Finalmente muito obrigado à UNICAMP e ao Brasil e a por me oferecer a oportunidade de viver uma experiência que me ajudou a crescer como pessoa e como profissional.

SÚMULA CURRICULAR

Andersson Alirio Acevedo Serrato

Geólogo pela "Universidad Nacional de Colombia", sede Bogotá (2011).
Possuo experiência na área de Metalogênese, com ênfase em geologia de campo, caracterização e evolução de depósitos do tipo pórfiro, epitermal e orogênicos, usando petrografia, estudos de inclusões fluidas, isótopos estáveis e geoquímica mineral. Trabalhei em 2011 no sul da Colômbia como geólogo de exploração mineral na prospecção de ouro. Assim mesmo durante este mesmo ano trabalhei no Chile como geólogo de projeto na prospecção de depósitos do tipo IOCG.
Em 2011, ingressei no Programa de Pós-Graduação em Geociências na modalidade de Mestrado pela Universidade Estadual de Campinas, com orientação do Prof. Dr. Roberto Perez Xavier. As atividades de pesquisa no mestrado têm se concentrado principalmente em depósitos de ouro que ocorrem hospedados em terrenos plutôno-vulcânicos da Província Aurífera de Alta Floresta (MT).

UNIVERSIDADE ESTADUAL DE CAMPINAS
INSTITUTO DE GEOCIÊNCIAS

GEOCRONOLOGIA E EVOLUÇÃO DO SISTEMA HIDROTERMAL DO DEPÓSITO AURÍFERO DE JURUENA, PROVINCIA AURÍFERA DE ALTA FLORESTA (MT), BRASIL

RESUMO

Dissertação de Mestrado
Andersson Alirio Acevedo Serrato

O depósito aurífero de Juruena localiza-se no setor oeste da Província Aurífera de Alta Floresta, sul do Cráton Amazônico, onde se hospeda em rochas graníticas da Suíte Intrusiva Paranaíta (1819 – 1793 Ma). Foram reconhecidos cinco tipos de alteração hidrotermal no depósito, organizados cronologicamente do evento mais precoce ao mais jovem: (1) alteração potássica com veios de quartzo-sulfetos e quartzo+clorita+fluorita+sulfetos; (2) alteração sericitica com veios de quartzo+molibdenita±pirita com halo de feldspato K e veios de quartzo+calcita+clorita com halo de sericita ; (3) carbonatação com veios de calcita-fluorita-sulfetos; (4) silicificação, pervasiva e em veios; e (5) alteração propilítica com veios de epídoto e calcita. A mineralização encontra-se hospedada nos eventos 1 e 3, onde aparece principalmente como inclusões ou preenchendo fraturas em pirita e também relacionado com fases minerais ricas em Te-Bi-Ag.

Estudos da paragênese do minério combinados com análises de microssonda, indicam sucessivos eventos de formação de pirita, definidos em quatro gerações: pirita euedral porosa (py1), desenvolvida nos veios iniciais da alteração potássica; pirita de granulação grossa, arredondada a subhedral, não porosa (py2), representante da segunda geração de pirita com cristais ocorrendo distribuídos na alteração potássica e sericitica; pirita anedral, muito porosa, com abundantes inclusões de silicatos, sendo esta fase dominante na alteração sericitica (py3). Pirita sobrecrescida nos cristais da geração mais jovem (py3), representante portanto da ultima geração. Ressalta-se ainda que as gerações de py2 e py3 contêm inclusões de ouro livre e ouro-teluretos. A geoquímica de elementos-traço em pirita revela que pirita de estágios mais precoces (py1) geralmente é mais pobre em ouro (Au < 0.02wt%) quando comparada à pirita de fases mais tardias (py2 e py3) que podem mostrar valores de Au de até 0.035 wt%. As análises também sugerem que o ouro deve ocorrer como nano- micropartículas na pirita e não como parte de sua estrutura cristalina. O cobre apresenta comportamento oposto, com concentrações mais baixas em pirita tardia (Cu < 0.04wt%).

Uma amostra de molibdenita associada à paragênese do minério aurífero forneceu uma idade modelo Re-Os de 1805 ± 7 Ma. Levando em consideração o erro, esta idade se sobrepõe parcialmente às idades U-Pb SHRIMP em zircão de 1790 ± 6.4 Ma,(com um nível de confiança de 95%, MSWD = 4.8, n =15) e de 1792 ± 5.8 (com um nível de confiança de 95%, MSWD = 0.32, n =17) obtidas, respectivamente em biotita monzogranito (principal hospedeira da mineralização) e em micromonzogranito representante da

última fase granítica no depósito. Essa sobreposição sugere uma possível relação genética entre o magmatismo félsico de idade correlata ao da Suíte Intrusiva Paranaíta e a mineralização aurífera.

Dados de inclusões fluidas indicam que fluidos aquo-carbônicos com salinidades entre 0.6 e 11.3 wt% NaCl equiv. e temperaturas no intervalo de 341 – 456 ^{o}C foram responsáveis pelos estágios iniciais da mineralização aurífera na alteração potássica. Durante a evolução os fluidos ricos em CO_2 decrescem, dando lugar para um regime de fluidos aquosos de salinidade elevada (31.4 e 36 wt% NaCl equiv.) com temperaturas entre 185 e 264 ^{o}C, representado por inclusões fluidas saturadas em sais. Fluidos essencialmente aquosos mais frios (155 – 285 ^{o}C) e de baixa salinidade representam os estágios finais do sistema hidrotermal.

Valores calculados de $\delta^{18}O$ para os fluidos hidrotermais variam de 6.9 e 0.5 ‰ indicando uma fonte predominantemente magmática, com adição de pequenas quantidades de aguas meteóricas nos veio mais tardios da alteração sericitica. Os valores $\delta^{34}S$ para os sulfetos (-7.1 até +1.5 ‰) são consistentes com a precipitação a partir de uma fonte magmática oxidada. Um importante zoneamento foi reconhecido: valores menores de $\delta^{34}S_{sulfetos}$ (-7.1 até -4.5 ‰) tendem a se associar aos veios representativos do estágio precoce da mineralização aurífera, enquanto que valores mais elevados de $\delta^{34}S_{sulfetos}$ (-0.5 até +1.5 ‰) correspondem ao sulfetos contidos na carbonatação, o ultimo evento estudado. Este zoneamento é o resultado da interação fluido-rocha que muda as condições de oxidação-redução ao longo da evolução do fluido magmático-hidrotermal no depósito.

Baseados nos dados de campo, petrográficos, de inclusões fluidas, isotópicos e na geoquímica de elementos traço é possível definir que o depósito aurífero de Juruena se trata de um sistema magmático-hidrotermal, com fluidos ricos em CO_2 que evoluem para fluidos aquosos. O minério foi depositado diretamente dos fluidos hidrotermais durante diferentes e repetidos pulsos hidrotermais de composição variável. Os processos de formação do depósito aurífero de Juruena são similares aos depósitos do tipo ouro-pórfiro.

Palavras chaves: Depósito Aurífero de Juruena, Geocronologia, Isótopos Estáveis, Inclusões Fluidas, Elementos Traço

UNIVERSITY OF CAMPINAS
INSTITUTE OF GEOSCIENCES

THE EVOLUTION OF THE PALEOPROTEROZOIC JURUENA INTRUSION-HOSTED GOLD DEPOSIT, NORTHWESTERN SECTOR OF THE ALTA FLORESTA GOLD PROVINCE (MT), BRAZIL.

ABSTRACT

Masters Degree

Andersson Alirio Acevedo Serrato

The Juruena deposit belongs to a large group of intrusion-hosted gold deposits of the Alta Floresta Gold Province in the southern portion of the Amazonian Craton. This gold deposit is hosted by granitic rocks of Paranaita Intrusive Suite (1819 to 1793 Ma) which is crosscut by different sets of mafic intrusions. The hydrothermal alteration can be divided into five stages, from early to late: (1) potassic alteration, with quartz+sulfides and quartz+chlorite+fluorite+sulfides veins (2) sericitic alteration with quartz+molybdenite±pyrite veins with K-feldspar halo and quartz+calcite+chlorite veins with sericitic halo; (3) carbonatization with calcite+fluorite+sulfides veins; (4) silicification, pervasive and in veins; and (5) propylitic alteration with epidote and calcite veins. The mineralization is hosted in stages 1 and 3, where it occurs mostly as particles or filling fractures in the pyrite crystals and related with Te-Bi-Ag phases.

Paragenetic studies of the mineralization combined with microprobe analysis indicated successive stages of pyrite formation defined in four generations: euhedral porous form the earliest generation, developed in the earliest veins from potassic alteration (py1). Coarser grained pyrite is a rounded to subhedral nonporous generation distributed in potassic and sericitic alterations (py2). Anhedral very porous generation contains abundant inclusions of silicates and is the dominant generation on the sericitic alteration (py3). Py2 and py3 contain inclusions of native gold and gold tellurides. The fourth generation (py4) overgrows the earlier py3. The geochemistry of trace elements in pyrite reveal that the earliest generation (py1) is particularly depleted in Au (Au $\leq$ 0.02 wt%) in comparison with other pyrite generations (py2 and py3) that showed results up to 0.35 wt% Au. Microprobe analysis also suggests that gold occurs mostly as nano- micro-size particles in the pyrite, and not as part of its crystal structure. Copper presents opposite behavior, with the lowest concentration on the richest gold pyrites (Cu $\leq$ 0.04 wt%.).

A sample of molybdenite coexisting with Au-bearing pyrite from stage 2, revealed a Re-Os model age of 1805 ± 7 Ma. Taking into account the uncertainties, this age could overlaps with the U/Pb SHRIMP obtained in zircon from granitic rocks of the Paranaíta Intrusive Suite at 1790 ± 6.4 Ma (95% confidence level, MSDW= 4.8, n = 15) and 1792 ± 5.8Ma (95% confidence level, MSDW = 0.32, n = 17). This poses a genetic relationships between the felsic magmatism attributed to this granitic suite and the emplacement of the gold mineralization at the Juruena deposit, which can be defined as the result of a magmatic-hydrothermal system.

Fluid inclusions microthermometric data obtained in veins of quartz constrain the formation of the early mineralizing events in the range of 341 and 456 oC from a low to moderate-salinity (0.6 and 11.3 wt% NaCl equiv.) H_2O-CO_2-NaCl fluid. At late stages of gold mineralization, fluid gradually become CO_2-poor and higher salinities (31.4 to 36 wt% NaCl equiv.), represented by NaCl-bearing fluid inclusions. More diluted (0.4 to 13.7 wt% Nacl equiv.) and cooler (185 to 285 ^oC) aqueous fluid inclusions dominate the latest stages of the magmatic-hydrothermal system.

Calculated $\delta^{18}O_{fluid}$ values range from 6.9 to 0.5 ‰ indicating that ore fluids of essentially magmatic origin in the earlier mineralizing stages undergoes mixing with meteoric waters in the late stages. Sulfides from early veins display $\delta^{34}S_{Sulfide}$ values in the range of -7.1 to -4.5 ‰, whereas more enriched $\delta^{34}S_{Sulfide}$ values varying from -0.5 to +1.5 ‰ are obtained in sulfides from the late veins sets. The more negative $\delta^{34}S_{Sulfide}$ values may reflect sulfides precipitation from oxidized magmatic fluids in the early ore stages, whereas higher $\delta^{34}S_{Sulfide}$ values be attained in later stages as a result of water-rock interactions, fluid mixing and change of the redox conditions.

Based on field, petrography, fluid inclusions, isotopic evidence and geochemistry of trace elements in pyrites, is possible to define that Juruena gold deposits is a magmatic-hydrothermal system, with hot CO_2-fluid rich that evolve to lower temperature, aqueous fluids. The gold was precipitated directly from the hydrothermal solution during different pulses. The formation processes of the Juruena gold deposit are most similar with a typical small Au-porphyry system formed in the Paleoproterozoic.

Keywords: Juruena Gold Deposit, Geochronology, Stable Isotopes, Fluid Inclusions, Trace elements

SUMÁRIO

LISTA DE FIGURAS

LISTA DE TABELAS

Anexo: The Evolution of the Paleoproterozoic Juruena Intrusion-Hosted Gold Deposit, Northwestern Sector of the Alta Floresta Gold Province (MT), Brazil.

1. INTRODUÇÃO

A Província Aurífera de Alta Floresta (PAAF), também conhecida com Província Aurífera Juruena-Teles Pires (Silva & Abram, 2008), encontra-se localizada na porção sul do Cráton Amazônico e consiste essencialmente de sequências plutono-vulcânicas interpretadas como de arcos continentais desenvolvidos durante o Paleoproterozóico (2,0 Ga – 1.75 Ga;). No modelo de Santos et al. (2000) a PAAF encontra-se localizada nos limites da Províncias geocronológicas Tapajós-Parima (2.03 – 1.88 Ga) e Rôndonia-Juruena (1.82 – 1.54) (Fig.2). É estimado que de 1980 até 1999 a PAAF pode ter produzido até 5.3 milhões de onças de ouro provenientes de diferentes depósitos primários (filonares) e aluvionares, em particular no seu segmento leste (Paes de Barros. 2007).A grande maioria destes depósitos têm sido lavrados de forma artesanal por garimpeiros.

Vários trabalhos de cunho metalogenético desenvolvidos na PAAF têm tido como foco a melhor definição das principais caraterísticas dos depósitos auríferos explotados, assim como a elaboração de um modelo genético adequado e que tenha implicações na exploração de ouro na província. Em geral, nos limites das zonas mineralizadas, sericita/muscovita, alteração potássica com feldspato K e alteração sódica pobremente desenvolvida e localmente pervasiva correspondem aos tipos de alteração hidrotermal caraterísticos nos depósitos melhor documentados da PAAF (Moura et al., 2006; Paes de Barros, 2007; Assis, 2011). As zonas mineralizadas frequentemente mostram associação espacial com alteração dominada por sericita/muscovita e são caraterizadas por conterem pirita ± calcopirita ± galena ± hematita e fases com Bi-Te-Ag-Mo. A grande maioria dos depósitos encontram-se hospedados em rochas graníticas relativamente oxidadas, cálcio-alcalinas a sub-alcalinas, metaluminosas a peraluminosas, de médio a alto potássio e mais subordinadamente em sequências vulcânicas/vulcanoclásticas (Paes de Barros, 2007; Assis, 2011). Baseado no estilo de mineralização, alteração hidrotermal, paragênese do minério e caraterísticas geoquímicas, as mineralizações auríferas podem ser divididas em dois grupos: (1) disseminada (e.g., depósitos Serrinha, Luizão, X1 e Pé Quente) e (2) depósitos em veios controlados estruturalmente (e.g., depósitos de Paraíba e Buriti).

Embora sejam reconhecidas caraterísticas similares entre os diferentes depósitos de ouro na PAAF, principalmente na sua porção leste, até o presente momento não foram completamente reconhecidos os mecanismos relacionados com a gênese dos depósitos, incluindo a origem das

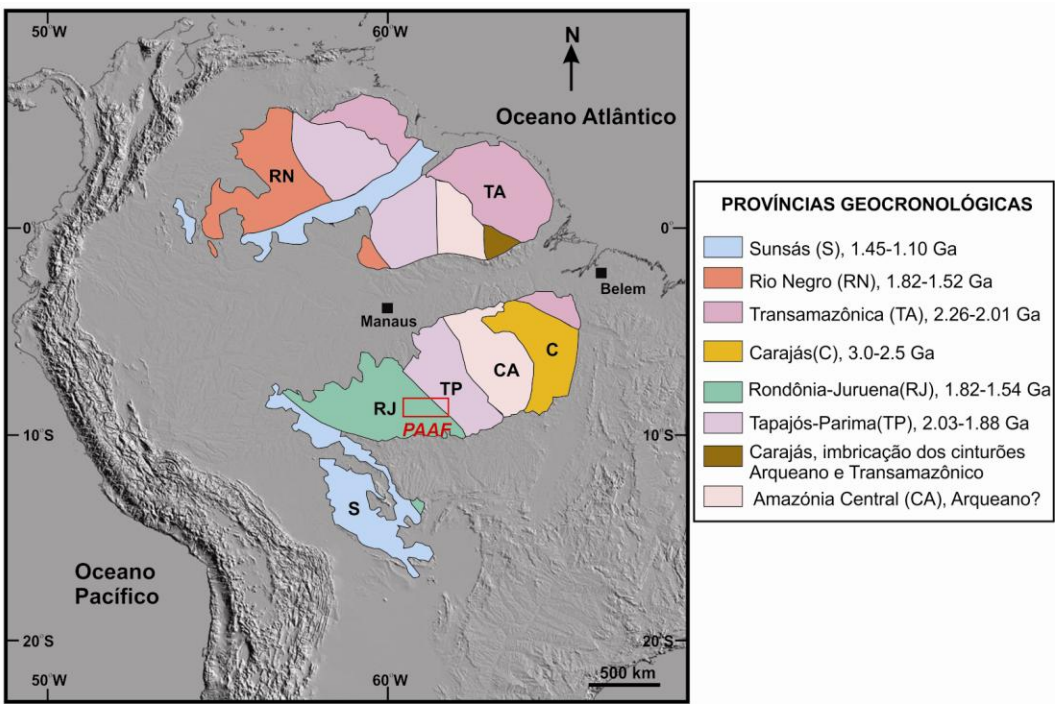

Figura 1. Mapa geológico do Cráton Amazônico mostrando as províncias geocronológicas e a localização da Província Aurífera de Alta Floresta (PAAF; retângulo vermelho) (modificado de Santos et al., 2000)

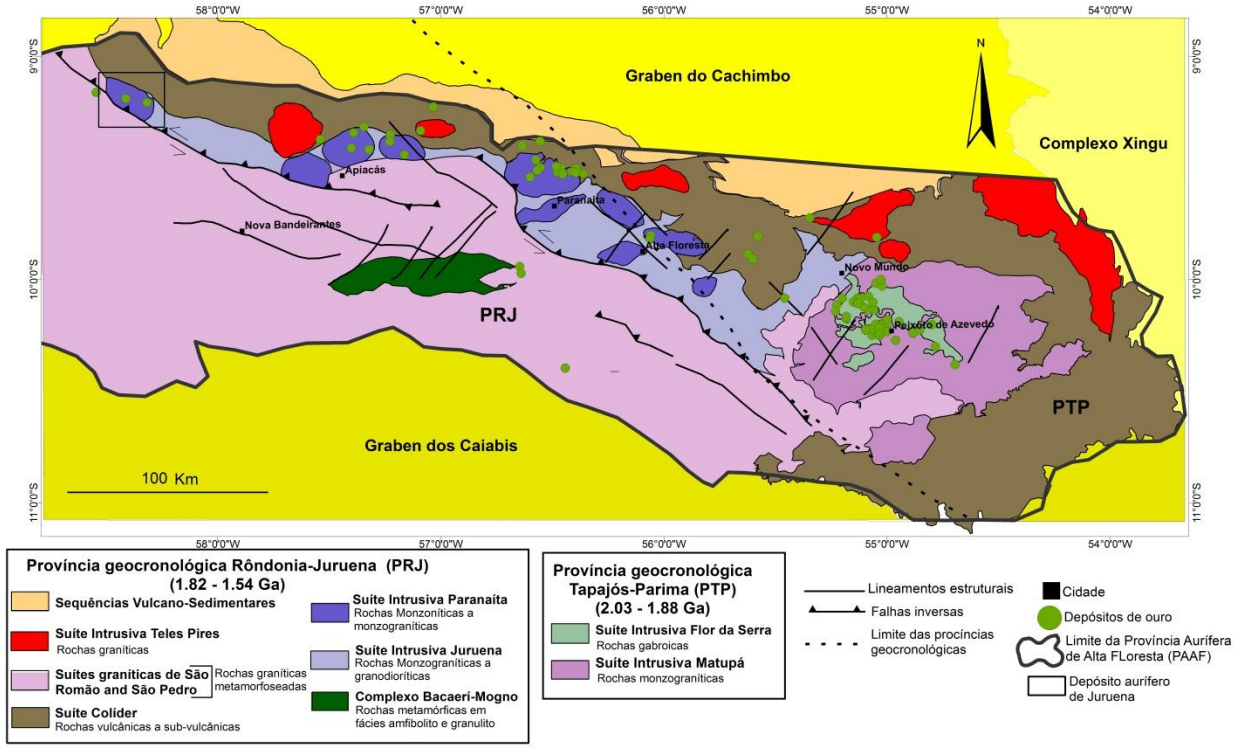

Figura 2. Mapa geológico regional da Província Aurífera de Alta Floresta (PAAF), mostrando o limite aproximado entre as Províncias Geocronológicas Tapajós-Parima e Rondônia-Juruena de acordo com Duarte et al. (2012). A localização do depósito aurífero de Juruena está ilustrada pelo quadrado no lado esquerdo da figura (Modificado de Souza et al., 2005).

fontes dos fluidos mineralizantes e a relação temporal da mineralização com as rochas graníticas hospedeiras.

A grande maioria dos estudos abordando os depósitos auríferos da província têm sido desenvolvido na porção leste da mesma. A investigação desses depósitos é de grande relevância ao estudo metalogenético da PAAF com o objetivo de se estabelecer ou descartar uma possível relação genética e temporal entre eles

O depósito aurífero de Juruena é, possivelmente, o principal depósito aurífero localizado no setor oeste da PAAF (Fig.2). Este depósito possui uma clara relação espacial com as rochas graníticas que hospedam a mineralização. As rochas hospedeiras, por sua vez, apresentam intensa alteração hidrotermal bem como caraterísticas mineralógicas similares quando comparado com os depósitos mais bem estudados da porção leste da província, tornando o depósito aurífero de Juruena de grande interesse no entendimento do contexto metalogenético regional.

Este trabalho apresenta os dados geocronológicos U-Pb (SHRIMP) em zircão das rochas graníticas e Re-Os de molibdenita relacionada com o minério aurífero. Também são expostos dados de isótopos de oxigênio e enxofre, inclusões fluidas e resultados de elementos traço em pirita. Com base dos dados obtidos, propõe-se um modelo genético para a formação do depósito aurífero de Juruena.

2. OBJETIVOS

Este projeto tem como objetivo determinar a evolução temporal do sistema hidrotermal responsável pela formação da mineralização aurífera do depósito de Juruena, incluindo os processos genéticos envolvidos na precipitação do minério e o papel do magmatismo félsicos. Para isso, os estudos nesse trabalho concentraram-se na definição (1) dos principais litotipos graníticos hospedeiros; (2) dos tipos e distribuição da alteração hidrotermal; (3) das idades de cristalização das rochas graníticas hospedeiras (Suíte Intrusiva Paranaíta) e da mineralização; e (4) das possíveis fontes e caraterísticas dos fluidos responsáveis pela mineralização.

3. PROVINCIA AURÍFERA DE ALTA FLORESTA

A Província Aurífera de Alta Floresta (PAAF) foi gerada durante a evolução do arco magmático, denominado por Souza et al. (2005) como Arco Magmático Juruena (1.85 – 1.75 Ga), regionalmente parte da Província Geocronológica Rondônia-Juruena. Este arco magmático é acrescionário à Província Tapajós – Parima (Santos et al., 2000). Na PAAF a Província Tapajós – Parima encontra-se representada pelas rochas graníticas pouco deformadas, geradas num ambiente pós-colisional da Suíte Intrusiva Matupá (1872 ± 12 Ma; Fig. 2) e pelas rochas básicas, de ambiente continental intraplaca, da Suíte Intrusiva Flor da Serra (1879 ± 15 Ma; Fig. 2) (Souza et al., 2005; Silva e Abram, 2008).

A orogênese convergente que originou o Arco Magmático de Juruena teve um início em aproximadamente 1820 Ma. Movimentos compressivos desde o SW até NE deslocam uma crosta oceânica (Complexo Bacaerí-Mogno) na direção de uma área cratonizada, Arco Magmático Tapajós, resultando na subducção e consumo de placa oceânica. (Duarte et al., 2012). No Arco Magmático Juruena o embasamento é formado por rochas metamórficas de fácies amfibolito e granulito que compõem o Complexo Bacaerí-Mogno (não datado). Sequências plutono-vulcânicas encontram-se encaixadas no embasamento, compreendendo as seguintes unidades: Suíte Intrusiva Juruena (1848 - 1823 Ma), Suíte Intrusiva Paranaíta (1819 - 1793 Ma), e Suíte Colíder (1786 até 1781 Ma) (Souza et al., 2005; Santos et al., 2008). Unidades metamorforfizadas são descritas na província, representadas pelos Granitos São Romão (~ 1770 Ma) e Granito São Pedro (~1784 Ma). Granitos pós-colisionais da Suíte Intrusiva Teles Pires (1756 ± 16 Ma) representam as unidades graníticas mais jovens da PAAF. O Grupo Beneficiante (1700 – 1400 Ma) e a Formação Dardanelos (~ 1400 Ma), unidades vulcanossedimentares, completam a estratigrafia da província (Fig. 2).

4. METALOGÊNESE DO OURO NA PROVÍNCIA AURÍFERA DE ALTA FLORESTA

A metalogênese na PAAF tem sido um tópico muito discutido nos últimos anos. Em geral, diversas hipóteses têm sido propostas para explicar os processos que deram origem à mineralização aurífera na província, porém caraterísticas similares entre os diferentes depósitos têm sido reconhecidas que sugerem a hipótese que processos genéticos similares formaram os depósitos auríferos nesta área.

A mineralização encontra-se relacionada a rochas graníticas do tipo I relativamente oxidadas, cálcio-alcalinas a sub-alcalinas, metaluminosas a peraluminosas de alto potássio, geradas em ambiente de arco vulcânico (Paes de Barros, 2007; Assis, 2011). A alteração hidrotermal é caraterizada por zonas com alteração potássica com feldspato K, seguida por zonas com sericita/muscovita e finalmente alteração propilítica (Moura et al., 2006; Paes de Barros, 2007; Assis, 2011; Miguel-Jr, 2011; Rodrigues, 2012). As zonas mineralizadas estão frequentemente associadas à alteração dominada por sericita/muscovita (e.g., depósitos de Serrinha: Moura et al., 2006; Pé Quente: Assis, 2011; X1: Rodrigues, 2012), e são caraterizados por conterem pirita calcopirita, concentrações subordinadas de galena, hematita e fases com Bi-Te-Ag-Mo. Estudos de inclusões fluidas sugerem a mistura de fluidos aquo-carbônicos coexistindo com fluidos aquosos de salinidade variada (Moura et al., 2006; Rodrigues, 2012). Dados de isótopos de enxofre, oxigênio e hidrogênio sugerem uma fonte magmática para os fluidos responsáveis pela mineralização (Moura et al., 2006).

Em conformidade com as caraterísticas mencionadas anteriormente, os depósitos minerais na PAAF têm sido comparados, quanto ao processo de formação, com depósitos do tipo ouro pórfiro e depósito do tipo *"Intrusion Related Gold Deposit",* sendo o primeiro o modelo mais aceito para explicar mineralização aurífera na província.

Com base na estreita relação entre as rochas graníticas e a mineralização e também em dados geocronológicos, foi proposto que a metalogênese do ouro no setor leste da província deve ter ocorrido em pelo menos 2 etapas (Paes de Barros, 2007; Silva e Abram, 2008; Miguel-Jr, 2011): (1) 1.98 – 1.95 Ga (e.g., depósitos Luizão e Edu: Paes de Barros, 2007; Pé Quente: Miguel-Jr, 2011); (2) 1.87 – 1.85 Ga (e.g., Serrinha: Moura, 1998). Estudos recentes fornecem novos dados sob a idade da mineralização na PAAF. Xavier et al. (2013) apresenta idade média Re-Os em pirita de 1786 ± 4 Ma para os depósitos Luizão e Pé Quente, assim como uma idade média Re-Os em molibdenita de 1786 ± 7 Ma para o depósito X1. Esses dados são concordantes como a

idade Ar-Ar de 1786 ± 14 Ma, obtida na alteração hidrotermal num Garimpo hospedado no Granito Nhandu (1889 Ma; Silva e Abram, 2008). Com base na informação anterior, é proposto que as mineralizações nos depósitos da PAAF poderiam estar relacionadas a um único evento magmático-hidrotermal desenvolvido no intervalo entre 1782 – 1792 Ma, e não durante diferentes eventos magmáticos (Xavier et al., 2013).

5. MATERIAIS E MÉTODOS

Para a execução desta pesquisa foi realizado um trabalho de campo de 21 dias, entre os dias 2 e 22 de Junho de 2013, onde foram reconhecidas as caraterísticas das rochas hospedeiras e os tipos e distribuição da alteração hidrotermal através da descrição detalhada de 7 furos de sondagem, que apresentaram os melhores teores de ouro no depósito. Estas observações foram complementadas posteriormente com ajuda de estudos petrográficos em luz transmitida e refletida, e também com o auxilio do Microscópio Eletrônico de Varredura do Instituo de Geociências da Universidade Estadual de Campinas, obtendo assim, a evolução paragenética do minério.

5.1 U-Pb SHRIMP

Duas amostras das rochas graníticas hospedeiras foram selecionadas para as analises U-Pb em zircão através do método *"Sensitive High Resolution Ion Microprobe – SHRIMP"*. As amostras foram coletadas do biotita monzogranito (principal hospedeiro da mineralização) e do micromonzogranito que corta a mineralização. Os concentrados de zircão foram extraídos usando os métodos gravimétricos e magnéticos convencionais:(1) britagem; (2) moagem; (3) peneiramento em peneiras de nylon de 250 µm de abertura; (4) bateamento manual; (5) separação através de separador isodinâmico Frantz; e (6) separação manual dos grãos de zircão. As análises U-Pb em zircão foram feitas no Centro de Geocronologia da Universidade de São Paulo.

5.2 Geocronologia Re-Os em molibdenita

Uma amostra de molibdenita associada à paragênese do minério aurífero foi analisada para se determinar a idade da mineralização. A amostra estudada foi coletada do alvo Uiliam. Esta análise foi feita no Laboratório de Isótopos Radiogénicos do Departamento de Ciências Atmosféricas e da Terra da Universidade de Alberta (*Radiogenic Isotope Faccility of the Department of Earth and Atmospheric Sciences, University of Alberta)*, Canada.

5.3 Microtermometria

As análises de inclusões fluidas foram realizadas em quatro amostras bipolidas provenientes de veios de quartzo que representam os diferentes eventos de formação do depósito mineral: (1) veio de quartzo-sulfeto-ouro hospedados na alteração potássica; (2) veio de quartzo-clorita±pirita também hospedado na alteração potássica; (3) veio de quartzo-molibdenita-pirita com halo de feldspato-K hospedado na alteração sericítica; e (4) veio de quartzo-pirita com halo sericitico

hospedados na alteração com sericita. Estudos petrográficos foram realizados com o objetivo de identificar os tipo e caraterísticas das inclusões presentes em cada uma das amostras.

Para as análises de microtermometria utilizou-se uma platina de aquecimento-resfriamento LINKAM THMSG 600 adaptada a um microscópio convencional LEICA® DMLP, no Laboratório de Microtermometria do IG/Unicamp.

5.4 Isótopos Estáveis

Os estudos de oxigênio e enxofre foram feitos no Serviço Geológico dos Estados Unidos (*United State Geologcal Survey – USGS*), Denver, Colorado.

5.4.1 **Isótopos de Enxofre:** Um total de 13 amostras de pirita (9) e calcopirita (7), foram analisadas usando o método descrito por Giesemann et al., (1994). Os sulfetos foram extraídos de veios de quartzo sulfetados relacionados com a alteração potássica e alteração sericitica assim como de veio de calcita-sulfetos presentes na alteração com carbonato. Os cristais de pirita e calcopirita foram concentrados manualmente em lupa binocular com o objetivo de se obter concentrados puros. Posteriormente os sulfetos foram pesados dentro de uma capsula de estanho misturados com pentóxido de vanádio e posteriormente levados no CE Elantech Inc. Flash 2000 Elemental Analyzer acoplado a um espectrômetro de massa ThermoFinnigan Delta Plus XP ™ de fluxo continuo. Os dados são reportados na notação δ em comparação com o padrão de referencia "*Vienna Canyon Diablo Troilite*" (V-CDT).

5.4.2 **Isótopos de oxigênio:** No total, onze amostras de quartzo provenientes dos veios hospedados nas alterações potássica e sericitica foram analisadas. Os cristais de quartzo foram concentrados manualmente com o objetivo de garantir a pureza dos concentrados. As analises foram executadas a cabo seguindo o procedimento descrito por Clayton and Mayeda (1963), usando BrF5, com ajuda de linhas de extração. Os resultados obtido são expressados na notação δ em comparação com o padrão V- SMOV (*Standard Mid Ocean Water*).

5.5 Análise de Microssonda Eletrônica (Electron Probe Microanalysis EPMA)

Seis amostras dos veios de quartzo ricos em sulfetos foram selecionadas para a realização de EPMA. O primeiro passo foi mergulhar completamente as lâminas delgadas polidas no ácido nítrico durante 30 segundos (etching), com o objetivo de revelar as diferentes texturas dos cristais de pirita que às vezes são apagadas durante o processo de polimento. Posteriormente foram

desenvolvidos estudos petrográficos detalhado para identificar mudanças morfológicas, de textura e paragênese mineral dos cristais de pirita. Posteriormente durante a petrografia foram feitos mapas das lâminas com o objetivo de garantir que os cristais descritos na petrografia fossem os analisados por microssonda. As análises foram feitas em cristais de pirita em lâminas delgadas polidas usando uma microssonda modelo JEOL JXA-8900, equipada com cinco espectrómetros de dispersão de comprimento de onda. Este análise foram executadas no Serviço Geológico dos Estados Unidos, Denver, Colorado.

6. RESUMO DO ARTIGO

6.1 *"The Evolution of the Paleoproterozoic Juruena-Hosted Gold Deposit, Northwestern Sector of the Alta Floresta Gold Province, (MT), Brazil"*

Neste artigo são descritos os seguintes aspectos: (1) caraterísticas geológicas do depósito; (2) tipos e distribuição da alteração hidrotermal; (3) idade do magmatismo félsicos (U/Pb em zircão obtido por SHRIMP), e da mineralização (Re-Os em molibdenita); (4) evolução e fonte dos fluidos hidrotermais responsáveis pela mineralização aurífera; e (5) geoquímica de elementos traço em pirita.

O depósito aurífero de Juruena está localizado no setor noroeste da PAAF. Encontra-se relacionado espacial e temporalmente com rochas graníticas colocadas durante múltiplos pulsos magmáticos relacionados, possivelmente, com a evolução da Suíte Intrusiva Paranaíta (Fig. 2). O depósito de Juruena consiste em 6 alvos principais: Arrastro, Querosene, Jacaré Field, Noventa Graus, Uiliam e Crente, sendo os dois últimos, os corpos estudados neste trabalho (Fig. 3: mapa de Juruena).

Em geral as rochas graníticas hospedeiras apresentam composição homogênea com variações texturais e no conteúdo de biotita, principal mineral acessório. Estas rochas podem ser classificadas da mas precoce a mais jovem da seguinte forma: biotita monzogranito (principal hospedira da mineralização), biotita monzogranito porfirítico e micromonzogranito, todas elas cortadas por diques máficos de composição dolerítica.

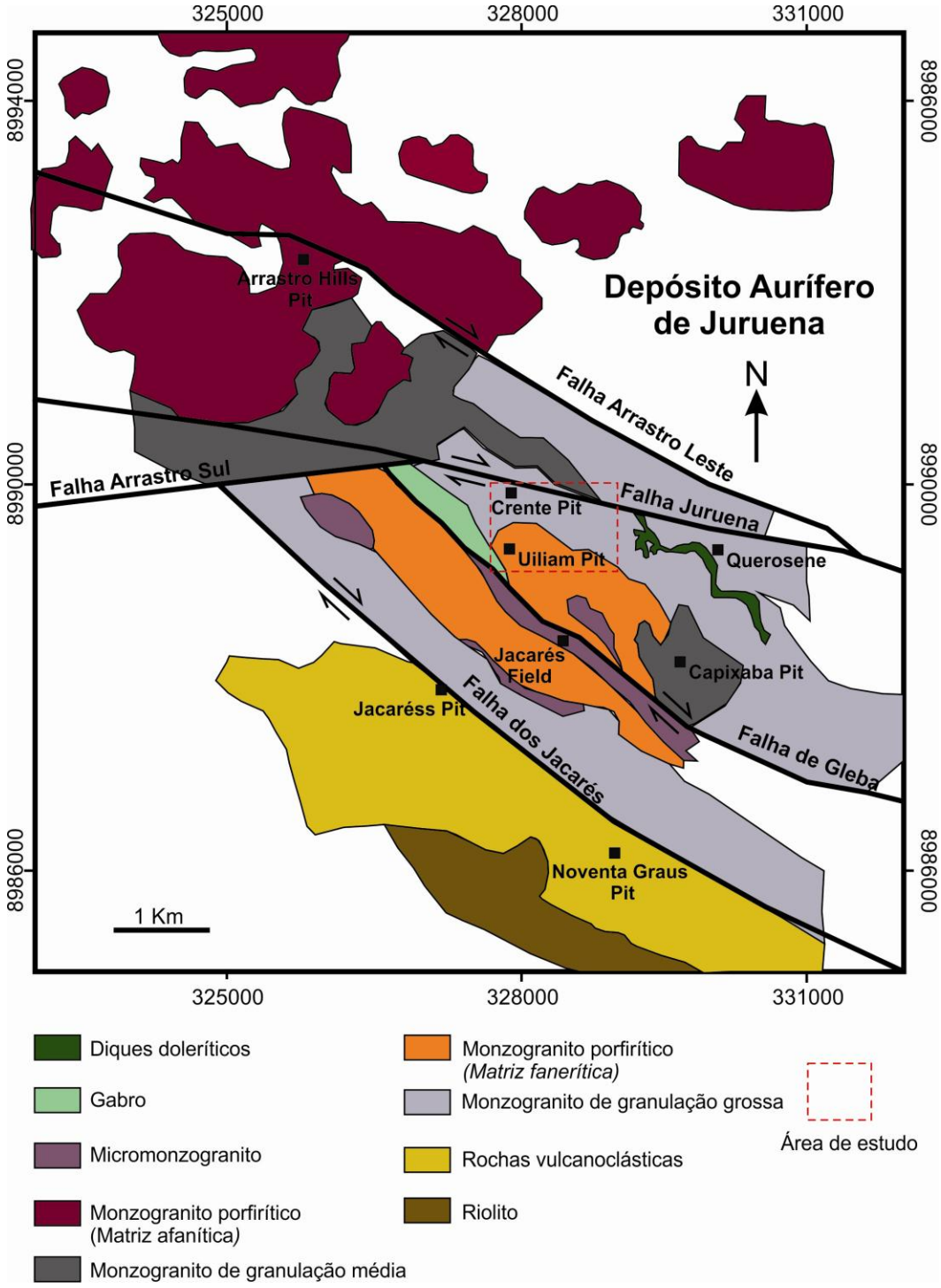

Figura 3. Mapa geológico generalizado do depósito aurífero de Juruena (modificado de Lago Dourado Ltda, 2011) O quadrado vermelho mostra os alvos estudados.

Cinco tipos de alteração hidrotermal foram identificados: (1) alteração potássica com feldspato K; (2) alteração sericitica com sericita-quartzo-pirita; (3) carbonatação, disseminada e em veios com sulfetos; (4) silicificação e (5) alteração propilítica com epídoto clorita e calcita, observada principalmente nos diques máficos.

Além disso, foram identificados veios de quartzo isolados relacionados exclusivamente a um tipo específico de alteração hidrotermal, já que veios que aparecem dentro de uma alteração especifica não se repetem em nenhuma outra. Estes veios segundo as caraterísticas morfológicas e a assembleia paragenética foram ordenados cronologicamente, levando em consideração que não foi possível observar relações de cortes entre eles. Neste trabalho este veios foram denominados como sub-eventos.

Na alteração potássica dois tipos de veios foram identificados: veios de quartzo-sulfeto apresentando calcopirita e pirita como componentes principais, e bornita-galena-teluretos como acessórios (sub-evento 1.1). O outro tipo de veio associado a esta alteração é composto por quartzo-clorita-fluorita-pirita. Na alteração sericitica veios de quartzo-molibdenita-pirita com halo de feldspato potássico caracterizam o sub-evento 2.1, enquanto que veios de quartzo-pirita tipicamente com halo sericitico foram definidos como o sub-evento 2.2.

O ouro encontra-se hospedado principalmente nos sub-eventos 1.1 e no evento 3. O minério aparece como ouro-livre nos cristais de pirita, preenchendo fraturas nos sulfetos e associado a teluretos na forma de pequenas partículas, também inclusas nas piritas. Ocasionalmente o ouro pode ocorrer também associado a sulfetos disseminados dentro da alteração sericitica.

6.2 Resultados

Os dados U-Pb em zircão fornecem uma idade de cristalização magmática entre 1790 ± 6.4 Ma para o monzogranito e 1792 ± 5.8 Ma para o micromonzogranito. O cálculo foi feito utilizando o diagrama da concórdia normal, com um nível de confiança de (1σ) 95%. Por outro lado, a idade Re-Os obtida em molibdenita associada à paragênese do minério aurífera foi de 1805 ± 7 Ma calculada com um nível de confiança de (2σ).

Os resultados dos isótopos de enxofre variam entre -7.8 ‰ e +1.5 ‰ em pirita, e entre -7.1 ‰ até -1.9 ‰ em calcopirita. Embora sejam identificadas pequenas variações isotópicas nos diferentes eventos estudados, foi possível observar que os veios dos eventos iniciais são isotopicamente mais leves em comparação com os sulfetos dos eventos tardios.

Quatro tipos de inclusões fluidas foram reconhecidos durante os estudos petrográficos dos veios de quartzo do depósito. Estas foram classificadas em: C50, B20, B20H e B15, donde a letra "B" denota *"bubble"* e o numero representa o volume médio que ocupa a bolha (vapor) dentro da inclusão. A letra "H" se refere á presença de cristais filhos de halita e a letra "C" representa as inclusões que contem gás carbônico (CO_2) junto com uma fase gasosa. Em todos os casos o tamanho das inclusões não foi maior do que 20 μm.

O tipo C50 esta presente, exclusivamente, no sub-evento 1.1, apresenta temperaturas de homogeneização entre 341 - 456 ^{o}C e salinidade entre 0.6 e 11.3 wt% NaCl. O tipo B20, dominante no sub-evento 1.2 presente ocasionalmente no sub-evento 2.1, têm salinidade variando entre 1.7 e 16.1 wt% NaCl, e temperaturas de homogeneização entre 280 e 385 ^{o}C. Algumas delas presentam clatratos indicando presença de CO_2. Os fluidos saturados em sais que geraam as inclusões do tipo B20H são pouco comuns, aparecem esporadicamente no sub-evento 1.2 e é mais comum no evento 2.1. Nestas inclusões o cristal de halita desaparece entre 185 e 264 ^{o}C fornecendo valores de salinidade que varia entre 31.4 e 36 wt% NaCl, a bolha homogeneizou-se no intervalo entre 239 e 349 ^{o}C. O ultimo tipo de inclusões (B15), domina o sub-evento 2.2 e ocasionalmente aparece no sub-evento 2.1, apresenta as menores temperaturas de homogeneização do sistema (185 – 285 ^{o}C) com salinidades entre 0.4 – 13.2 wt% NaCl.

Assumindo que os fluidos estavam em equilibrio com o quartzo, calculou-se o $\delta^{18}O$ para os fluidos mineralizantes, utilizando-se a equação de Clayton et al. (1972). Para isso foram usadas as temperaturas médias das inclusões fluidas dominantes em cada um dos eventos hidrotermais. Os valores obtidos variam entre 6.87 e 0.5 ‰, donde os valores mais altos estão relacionados aos eventos iniciais, enquanto que os valores próximos de zero estão associados ao evento mais tardio (sub-evento 2.2).

Quatro gerações de pirita foram diferenciadas (py1 até py4), levando-se em consideração as caraterísticas morfológicas, resposta dos cristais de pirita ao ataque com ácido nítrico (*etching)* e a paragênese mineral. A geoquímica de elementos traço mostrou que os principais elementos presentes em todas as gerações de pirita são o Ta, Cu e Au. Os maiores valores de Au encontraram-se nas piritas 2 e 3, enquanto que o Cu apareceu predominantemente nas piritas da primeira geração. O Ta apresenta um comportamento constante em todas as gerações enquanto que os valores de As e Sb foram constantes para cada amostra, com mudanças importantes em

alguns cristais, entretanto não foi possível estabelecer uma correlação entre estes elementos e o minério.

Análises na pirita euedral porosa da primera geração (py1) mostraram baixas concentrações nos elementos traços (As, Sb, Te e Au abaixo do limite de deteçao), enquanto que o Cu apareceu como o elemento principal (até 0.71 wt%). A segunda geração de pyrita (subedral sem poros) é mais rica em ouro (0.03 wt%). e diminui o conteúdo de Cu. O Cu nesta geração também diminuiu consideravelmente, enquanto que a concentração de Au aumenta A py3 (anaedral, muito porosa), apresenta os maiores valores de Au dos quatro tipos de pirita, no entanto, os outros elementos traço foram similares aos da py2. Na última geração de py (euedral a subedral), os teores de todos todos os elementos traço, em geral, diminuiu em relação às gerações anteriores, sendo o As o elemento que apresentou os teores mais constante quando comparado com as outras gerações.

7. DISCUSSÃO

Os resultados de U-Pb em zircão (1790 ± 6.4 e 1792 ± 5.8 Ma) das rochas hospedeiras, e a idade Re-Os em molibdenita (1805 ± 7 Ma), apresentam idades que poderiam ser correlacionáveis, levando em consideração o erro analítico destas técnicas. Além de que as idades obtidas da rocha hospedeira e da mineralização não apresentam uma clara sobreposição, a mineralização aurífera no depósito de Juruena pose ser relacionada com o magmatismo félsicos da Suíte Intrusiva Paranaíta (1819 – 1793 Ma; Santos et al., 2008).

Os dados de isótopos de enxofre mostram um aumento gradativo de $\delta^{34}S_{sulfeto}$, onde os valores mais baixos encontram-se relacionado aos veios mais precoces e os valores mais altos estão associados aos eventos finais que deram origem aos sulfetos na carbonatação. Este comportamento permite interpretar que os fluidos responsáveis pela mineralização são fluidos oxidados de origem magmática (Ohmoto and Rye, 1979). O enriquecimento progressivo em $\delta^{34}S$ desde os sulfetos contidos na alteração potássica até os sulfetos na carbonatação, não pode ser explicado simplesmente pela deposição dos sulfetos via resfriamento do fluido magmático-hidrotermal, já que o resfriamento produz uma tendência oposta (Rye, 1993). O enriquecimento progressivo em $\delta^{34}S$ é o resultado de um importante processo de redução dos fluidos iniciais, oxidados ricos em metais e sulfatos que aumenta com a distancia em relação ao centro da zona mineralizada, representada pelaalteração potássica, até as zonas mais distais, representada neste caso, na zona com carbonatação (Deyell, 2005; Wilson et al., 2007).

Dados de inclusões fluidas mostram que o depósito foi formado na sua etapa inicial por fluidos aquo-carbônico. Durante a evolução do sistema, os fluidos ricos em CO_2 decrescem, dando lugar a um regime de fluidos aquosos salinos e hipersalinos (B20 e B20H), ao mesmo tempo em que diminui a temperatura de homogeneização. Mudanças na temperatura de homogeneização, e não na salinidade, com exceção do tipo B20H, juntamente com a baixa concentração de CO_2 em quase todos os eventos hidrotermais, exceto nos fluidos relacionados à alteração potássica, é evidencia que os fluidos foram exsolvidos de uma única fonte, possivelmente de origem magmática-hidrotermal. Esta hipótese é comprovada pelos dados de isótopos de oxigênio, que indicam associação dos fluidos mineralizantes com uma fonte magmática (Taylor, 1979), com exceção dos fluidos de baixa temperatura (inclusões fluidas B15) que se formaram na parte final da alteração sericítica, e neste caso poderiam ser o resultado de uma fonte magmática pouco misturada com águas meteóricas (Taylor, 1979).

A origem do CO_2 em sistemas magmáticos foi estudada e descrita por Giggenbanch (1992), e Lowestern (2000, 2001). Estes autores sugerem que a presença de CO_2 promove a imiscibilidade das fases voláteis do magma bem como no fluido hidrotermal, processo que favorece a deposição do ouro em veios ricos em CO_2, formados durante o desenvolvimento da alteração potássica. De qualquer maneira, a presença de CO_2 têm sido relacionada com sistemas magmáticos profundos (Baker, 2002). Esta caraterística permite explicar a presença de fluidos aquo-carbônicos relacionados à mineralização em rochas graníticas, além de assegurar a não necessidade de fontes externas para explicar a presença deste tipo de fluidos.

Os resultados das análises de elementos traço em piritas não evidenciam uma clara relação entre os elementos analisados, mas foi possível definir caraterísticas importantes relacionadas à precipitação do ouro e os possíveis processos responsáveis pela sua deposição. O ouro encontra-se presente em todas as gerações de pirita, as principais concentrações estão nos cristais anedrais porosos (py3). Os elevados valores de ouro podem ser explicados em virtude de processo de dissolução-precipitação (Putnis, 2002), processo que favorece o transporte e posterior deposição dos elementos como nano– micropartículas, favorecido especialmente pela intensa interação dos fluidos hidrotermais. A relação entre ouro e arsênio têm sido identificada em diferentes depósitos minerais (e.g., *Carlyn-type*¸ depósitos epitermais e depósitos orogenéticos), onde foi comprovado que a substituição de As por S promove a deposição de ouro livre nos cristais de pirita (Cook et al., 2009). No depósito de Juruena, esta relação não foi reconhecida, indicando que o minério aurífero no depósito está principalmente como nano- micropartículas (Au^0; Reich et al., 2005). As elevadas concentrações de Cu podem ser explicadas pela presença de partículas de calcopirita visto que a correlação Fe *Versu*s Cu não apresenta uma tendência clara, correlação essa que deve ser negativa já que o Cu geralmente substitui o Fe;(Shimazaki and Clark, 1970; Schmid-Beurmann and Bente, 1995), e portanto a possibilidade de ter cobre dentro da estrutura química das piritas é pouco provável. A não correlação dos elementos mais a presença dos mesmos predominantemente como micropartículas dentro dos cristais de pirita sugerem que o minério foi precipitado diretamente de um fluido magmático, durante diversos pulsos hidrotermais.

8. GÊNESE DO DEPÓSITO

O depósito aurífero de Juruena pode ser classificado como um depósito do tipo pórfiro com base nas seguintes caraterísticas: (1) Mineralização hospedada em rochas graníticas hospedeiras; (2) Idade Re-Os (1805 ± 7 Ma) é consistente com as idades U-Pb (1790 ± 6.4 Ma e 1792 ± 5.8 Ma) das rochas graníticas, indicando uma relação temporal entre a mineralização e o magmatismo da Suíte Intrusiva Paranaíta; (3) Os tipo e distribuição das alterações hidrotermais, começando com alteração potássica, passando à alteração sericitica até alteração propilítica, caraterísticas similares às do depósito Mo-W Nannihu (Yang et al., 2012), e às dodepósito Cu-Mo-Au de Deixing (Hou et al., 2013); (4) A presença de veios similares aos reconhecidos nos principais depósitos deste tipo (e.g., Gustafson and Hunt, 1975; Sillitoe, 2000; Seedorf et al., 2005); (5) Presença de inclusões fluidas aquo-carbônicas e salinas, que apear de não serem muito comuns nos depósitos do tipo pórfiro, em estudos recentes têm sido reportado a presença destas em alguns exemplos destes depósitos (e.g., Rusk et al., 2008; Landtwing et al., 2010), sendo ainda mais comuns em depósitos tipo pórfiro formados em zonas colisionais e pós-colisionais (Richards et al., 2005; Tang et al., 2013; Yang et al., 2013); (6) Valores de isótopos de enxofre que permitem sugerir que os fluidos mineralizantes são de origem magmática oxidada com uma forte incidência redox ao longo da sua evolução, que gerou um zoneamento característico, também reconhecido no pórfiro alcalino Mt Polley (Deyell, 2005) e no distrito de Cadia (Wilson et al., 2007); (7) Valore de isótopos de oxigênio que sugerem fonte estritamente magmática, a magmática fracamente misturada com águas meteóricas, para os fluidos responsáveis pelo transporte e precipitação do minério como ocorre por exemplo, no depósito Bajo la Alumbrera (Ulrich et al., 2002); e no depósito aurífero de Serrinha (Moura et al., 2006); (8) Presença do ouro e cobre como micropartículas dentro dos cristais de pirita e a não correlação entre os elementos analisados que, sugerem que o minério se depositou diretamente de uma fonte magmática hidrotermal durante diversos eventos hidrotermais, comportamento similar ao observado em depósito do tipo pórfiro e epitermais (e.g., Deditius et al., 2011; Reich et al., 2013).

9. CONCLUSÕES

Com base nos dados apresentados concluí-se que:

O depósito aurífero de Juruena encontra-se hospedado nas rochas graníticas oxidadas do tipo I da Suíte Intrusiva Paranaíta (idade U-Pb de 1790 ± 6.4 e 1792 ± 5.8 Ma). A idade da mineralização é 1805 ± 7 Ma (Idade Re-Os em molibdenita). A estreita relação entre as rochas graníticas e a mineralização indicam uma clara relação entre estes eventos. Dados isotópicos (oxigênio e enxofre), sugerem uma fonte magmática para os fluidos inicias CO_2-H_2O-NaCl que originaram a mineralização, com adição de aguas meteóricas nos eventos finais do depósito. Durante a evolução do magma, houve um aumento do conteúdo de NaCl e diminuiu progressivamente os fluidos aquo-carbônicos, formando inclusões saturadas em sal e finalmente fluidos aquosos de baixa temperatura. O ouro ocorre principalmente nos veios de quartzo-sulfeto e calcita sulfeto relacionados com o sub evento 1.1 e 3 respetivamente. O minério se apresenta principalmente como nano- micro inclusões dentro dos cristais de pirita ou preenchendo fraturas dentro dos sulfetos. O estudo de elementos traços nas piritas não mostra uma relação clara entre os diferentes elementos estudados embora, seja possível sugerir que o ouro foi depositado diretamente do fluido magmático durante diversos pulsos hidrotermais que favoreceram a remobilização e precipitação do ouro e dos outros elementos.

Baseados nestas observações, os processo que deram origem ao depósito aurífero de Juruena se assemelha a depósitos do tipo pórfiro. Esta pesquisa ressalta a importância das rochas graníticas da Suíte Intrusiva Paranaíta, como uma unidade muito importante dentro da exploração de ouro na PAAF.

10. REFERÊNCIAS BIBLIOGRÁFICAS

Assis, R.R., 2011, Depósitos auríferos associados ao magmatismo granítico do setor lest da Provincia de Alta Floresta (MT),Craton Amazônico: tipologia das mineralizações, modelos genéticos e implicações prospetivas: Disertação de Mestrado, Instituo de Geociências, Universidade Estadual de Campinas, 456 p.

Clayton, R.B and Mayeda, T.K., 1963, The use of bromide pentafluoride in the extraction of oxygen from oxides and silicates for isotopic analysis: Geochemica and Cosmochimica Acta, v. 27. p. 43-72.

Clayton, R.N., O'Neil, J.R., and Mayeda, T.K., 1972, Oxygen isotope exchange between quartz and water: Journal of Geophysical Research, v. 77, p. 3057–3067.

Cook, N.J., Ciobanu, C.L., and Mao, J., 2009, Textural control and gold distribution in As-free pyrite from Dongping, Huangtuliang and Hougou gold deposits, north China Craton (Hebei Province, China): Chemical Geology, v.264, p. 101-121.

Deditius, A., Utsunomiya, S., Ewing, R.C., Chryssoulis, S.L., Venter. D., and Kesler, S.E., 2009, Decoupled geochemical behaviour of As and Cu in hydrothermal systems: Geology, v.37, p. 707-710.

Deyell, C.L., 2005, Sulfur isotope zonation at the Mt Polley alkalic porphyry Cu-Au deposit, British Columbia, Canada: Mineral Deposit Research: Meeting the Global Challenge, China, 18-21 August, Proceedings, p. 373-376.

Duarte, B.T., Rodrigues, B.J., Riveiro, E.P.S., and Scandolara, J.E., 2012, Tectonic evolution of the Juruena magmatic arc between the Aripuanâ and Juruena Rivers: nortwest Mato Grosso State, Brazil: Revista Brasileira de Geociências, v.42, p. 824-840.

Giesemann, A., Jager, H.J., Norman, A.L., Krouse, H.R., and Brand W.A., 1994, On line sulfure isotope determination using an elemental analyser coupled to a mass spectometer: Analytical Chemistry, v.66, p. 2816-2819.

Giggenbach, W.F., 1992, Isotopic shifts in waters from geothermal and volcanic systems along convergent plate boundaries and their origin: Earth and Planetary Science Letters, v. 113, p. 495–510.

Gustafson, L.B., and Hunt, J.P., 1975, The porphyry copper deposit at El Salvador, Chile: Economic Geology, v. 70, p. 857–912.

Hou, Z., Pan, X., Li, Q., Yang, Z., and Song, Y., 2013, The giant Dexing porphyry Cu–Mo–Au deposit in east China: product of melting of juvenile lower crust in an intracontinental setting: Mineralium Deposita, v.48, p.1019-1045.

Landtwing, M.R., Furrer, C., Redmond, P.B., Pettke, T., Guillong, M., Heinrich, C.A., 2010 The Bingham Canyon porphyry Cu–Mo–Au deposit. III. Zoned copper–gold ore deposition by magmatic vapor expansion: Economic Geology, v.105, p.91–118.

Lowenstern, J.B., 2000, A review of the contrasting behavior of two magmatic volatiles: Chlorine and carbon dioxide: Journal of Geochemical Exploration, v. 69–70, p. 287–290.

Lowestern, J.B., ——2001, Carbon dioxide in magmas and implications for hydrothermal systems: Mineralium Deposita, v. 36, p. 490–502.

Miguel, Jr.E., 2011 Mineralizações auríferas do lineamento Peru-Trairão, Provincia aurífera de Alta Floresta - MT: controle estrutural e idade U-Pb das rochas hospedeiras. Disertação de Mestrado, Instituo de Geociências, Universidade Estadual de Campinas, 86 p.

Moura, M.A., 1998, O maçiço granítico Matupá no depósito de ouro Serrinha (MT): petrologia, alteração hidrotermal e matalogenia: Tese de Doutorado, Instituto de Geociências, UNB, Brasília, 238 p.

Moura, M.A., Botelho, N.F., Olívio, G.R., Kyser, T.K. 2006, Granite-related Paleoproterozoic, Serrinha gold deposit, Southern Amazonia, Brazil: hydrothermal alteration, fluid inclusion and stable isotope constraints on genesis and evolution. Economic Geology, 101:585-605.

Ohmoto, H., and Rye, R.O., 1979, Isotopes of sulfur and carbon, in Barnes, H.L., ed., Geochemistry of hydrothermal ore deposits, 2nd ed.: New York, Jhon Wiley & Sons, p.509-567.

Paes de Barros, A. J., 2007 Granitos da região de Peixoto de Azevedo - Novo Mundo e mineralizações auríferas relacionadas - Provincia Aurífera Alta Floresta (MT).Unpublished Phd. Thesis, Campinas, Brazil. University of Campinas, 171 p.

Putnis, A., 2002, Mineral replacement reactions: from macroscopic observations to microscopic mechanisms: Mineralogical Magazine, v. 66, p. 689–708.

Reich, M., Deditius, A., Cryssoulis, S., Li, J.W., Ma, C.Q., Parada, M.A., Barra, F., and Mittermayr, F., 2013, Pyrite as record of hydrothermal fluid evolution in a porphyry copper system: a SIMS/EPMA trace element study: Geochemica et Cosmochimica Acta, v.104, p. 42-62.

Reich, M., Kesler, S.E., Utsunomiya, S., Palenik, C.S., Chryssoulis, S.L., Ewing, R.C., 2005, Solubility of gold in arsenian pyrite: Geochimica et Cosmochimca Acta, v. 69, p. 2781–2796.

Richards, J.P., Wilkinson, D., and Ullrich, T., 2005, Geology of the Sari Gunay epithermal gold deposit, Nortwestern Iran: Economic Geology, v. 101, p.1455-1496.

Rodrigues, R., 2012, Caracterização geológica e metalogenética do depósito X1 : Província Aurífera de Alta Floresta, região de Matupá (MT): Unpublished, M.Sc. Thesis, Campinas, Brazil, University of Campinas. 70 p.

Rusk, B.G., Reed, M.H., and Dilles, J.H., 2008, Fluid inclusions evidence for magmatic-hydrothermal fluid evolution in the porphyry copper-molybdenum deposit at Bute, Montana: Economic Geology, v. 103, p.307-334.

Rye, R.O., 1993, The evolution of magmatic fluids in the epithermal environment; the stable isotope perspective. Economic Geology, v. 88, p. 733-752.

Santos J.O.S, Rizzoto G.J., Potter P.E., McNaughton N.J., Matos R.S., Hartmann L.A., Chemale Jr F., Quadros M.E.S. 2008, Age and autochthonous evolution of the Sunsás Orogen in West Amazon Craton based on mapping and U–Pb geochronology: Precambrian Research, v.165, p.120-152.

Santos, J.O.S., Hartmann, L.A., Gaudette, H.E., Groves, D.I., McNaughton, N.J., Fletcher, I.R., 2000 A new understanding of the Provinces of the Amazon Craton based on integration of field mapping an U-Pb and Sm-Nd geochronology: Gondwana Research, v. 3, p. 453-488.

Schmid-Beurmann, P., and Bente, K., 1995, Stability properties of CuS_2–FeS_2 solid solution series pyrite type. Mineral. Petrology, v. 53, p. 333–341.

Seedorff, E., Dilles, J.H., Proffett, J.M., Jr., Einaudi, M.T., Zurcher, L. Stavast, W.J.A., Jhonson, D.A., and Barton, M.D., 2005, Porphyry deposits: Characteristics and origin of hypogene features: Economic Geology 100th Anniversary Volume, p. 251-298.

Shimazaki, H., and Clark, L. A., 1970, Synthetic FeS_2–$CuFe_2$ solid solution and fukuchilite-like minerals: Canadian. Mineral. v.10, p. 648–664.

Sillitoe, H.R., 2000, Gold-Rich Porphyry Deposits: Descriptive and genetical models and their role in the exploration and discovery: Society of Economic Geologist. SEG Reviews, v. 13, p. 315-345.

Silva, M.G., & Abram, M.B., 2008, Projeto metalogenia da Província Aurífera Juruena-Teles Pires, Mato Grosso Informe de Recursos Minerais, Programa Geologia do Brasil, CPRM-Serviço Geológico do Brasil, Goiânia, Série Ouro, no. 16, 212p.

Souza, J.P., Frasca, A.A.S., Oliveira, C.C, 2005, Província Mineral de Alta Floresta. Relatório Integrado, Serviço Geológico Brasileiro, CPRM. Brasília, 164p.

Tang, K.F., Li, J.W, Selby, D., Zhou, M.F., Bi, S.J., and Deng, X.D., 2013, Geology, mineralization, and geochronology of the Qianhe gold deposit, Xiong'ershan area, southern North China Craton: Mineralium Deposita, v. 48, p.729-747.

Taylor, H.P., 1979, Oxygen and hydrogen isotope relationships in hydrothermal mineral deposits, in Barnes, H.L., ed., Geochemistry of hydrothermal ore deposits, 2nd ed.: New York, Jhon Wiley & Sons, p.236-2777.

Ulrich, T., Günther, D., and Heinrich, C.A., 2002, The evolution of a porphyry Cu-Au deposit, based on LA-ICP-MS analysis of fluid inclusions: Bajo de la Alumbrera, Argentina: Economic Geology, v. 97, p. 1743-1774.

Wilson, A.J., Cooke, D.R., Harper, B,J., and Deyell, C.L., 2007, Sulfur isotopic zonation in the Cadia district, southeastern Australia: exploration significance and implications for the genesis of alkalic porphyry gold–copper deposits: Mineralium Deposita, v.42, p. 465-487.

Yang, Y. F., Li, N., and C, Y.J., 2012, Fluid inclusion study of the Nannihhu giant porphyry Mo-W deposit, Henan province, China: Implications for the nature of porphyry ore-fluid system formed in continental collision setting: Ore Geology Reviews, v.46, p.83-94.

Anexo:

The Evolution of the Paleoproterozoic Juruena Intrusion-Hosted Gold Deposit, Northwestern Sector of the Alta Floresta Gold Province (MT), Brazil.

Andersson A Acevedo, [1†,] Roberto P Xavier,[1] Erin E Marsh[2], Robert A Creaser[3]

[1] *Geoscience Institute, University of Campinas, SP, Brazil*

[2] *U.S. Geological Survey, Box 25046, MS-973, Denver Federal Center, Denver, Colorado, 80305*

[3]*Department of Earth and Atmospheric Sciences, University Alberta, Edmonton, Canada T6G 2E3*

The Evolution of the Paleoproterozoic Juruena Intrusion-Hosted Gold Deposit, Northwestern Sector of the Alta Floresta Gold Province (MT), Brazil.

ANDERSSON A ACEVEDO, [1†,] ROBERTO P XAVIER,[1] ERIN E MARSH[2], ROBERT A CREASER[3]

[1] *Geoscience Institute, University of Campinas, SP, Brazil*

[2] *U.S. Geological Survey, Box 25046, MS-973, Denver Federal Center, Denver, Colorado, 80305*

[3]*Department of Earth and Atmospheric Sciences, University Alberta, Edmonton, Canada T6G 2E3*

Abstract

The Juruena deposit belongs to a large group of intrusion-hosted gold deposits of the Alta Floresta Gold Province in the southern portion of the Amazonian Craton. This gold deposit is hosted by granitic rocks of Paranaita Intrusive Suite (1819 to 1793 Ma) which is crosscut by different sets of mafic intrusions. The hydrothermal alteration can be divided into five stages, from early to late: (1) potassic alteration, with quartz+sulfides and quartz+chlorite+fluorite+sulfides veins (2) sericitic alteration with quartz+molybdenite±pyrite veins with K-feldspar halo and quartz+calcite+chlorite veins with sericitic halo; (3) carbonatization with calcite+fluorite+sulfides veins; (4) silicification, pervasive and in veins; and (5) propylitic alteration with epidote and calcite veins. The mineralization is hosted in stages 1 and 3, where it occurs mostly as particles or filling fractures in the pyrite crystals and related with Te-Bi-Ag phases.

Paragenetic studies of the mineralization combined with microprobe analysis indicated successive stages of pyrite formation defined in four generations: euhedral porous form the earliest generation, developed in the earliest veins from potassic alteration (py1). Coarser grained pyrite is a rounded to subhedral nonporous generation distributed in potassic and sericitic alterations (py2). Anhedral very porous generation contains abundant inclusions of silicates and is the dominant generation on the sericitic alteration (py3). Py2 and py3 contain inclusions of native gold and gold tellurides. The fourth generation (py4) overgrows the earlier py3. The geochemistry of trace elements in pyrite reveals that the earliest generation (py1) is particularly depleted in Au (Au ≤ 0.02 wt%) in comparison with other pyrite generations (py2 and py3), that showed results up to 0.35 wt% Au. Microprobe analysis also suggests that gold occurs mostly as nano- micro-size particles in the pyrite, and not as part of its crystal structure. Copper presents opposite behavior, with the lowest concentration on the richest gold pyrites (Cu ≤ 0.04 wt%.).

Fluid inclusions microthermometric data obtained in veins of quartz constrain the formation of the early mineralizing events in the range of 341 and 456 ^{o}C from a low to moderate-salinity (0.6 and 11.3 wt% NaCl equiv.) H_2O-CO_2-NaCl fluid. At late stages of gold mineralization, fluid gradually become CO_2-poor and higher salinities (31.4 to 36 wt% NaCl equiv.), represented by NaCl-bearing fluid inclusions. More diluted (0.4 to 13.7 wt% Nacl equiv.) and cooler (185 to 285 ^{o}C) aqueous fluid inclusions dominate the latest stages of the magmatic-hydrothermal system.

Calculated $\delta^{18}O_{fluid}$ values range from 6.9 to 0.5 ‰, indicating that ore fluids of essentially magmatic origin in the earlier mineralizing stages undergoes mixing with meteoric waters in the late stages. Sulfides from early veins display $\delta^{34}S_{Sulfide}$ values in the range of -7.1 to -4.5 ‰, whereas more enriched $\delta^{34}S_{Sulfide}$ values varying from -0.5 to +1.5 ‰ are obtained in sulfides from the late veins sets. The more negative $\delta^{34}S_{Sulfide}$ values may reflect sulfides precipitation from oxidized magmatic fluids in the early ore stages, whereas higher $\delta^{34}S_{Sulfide}$ values be attained in later stages as a result of water-rock interactions, fluid mixing and change of the redox conditions.

A sample of molybdenite coexisting with Au-bearing pyrite from stage 2 revealed a Re-Os model age of 1805 ± 7 Ma. Taking into account the uncertainties, this age could overlaps with the U/Pb SHRIMP obtained in zircon from granitic rocks of the Paranaíta Intrusive Suite at 1790 ± 6.4 Ma (95% confidence level, MSDW= 4.8, n = 15) and 1792 ± 5.8Ma (95% confidence level, MSDW = 0.32, n = 17). This poses a genetic relationship between the felsic magmatism attributed to this granitic suite and the emplacement of the gold mineralization at the Juruena deposit, which can be defined as the result of a magmatic-hydrothermal system

Based on field, petrography, fluid inclusions, isotopic evidence and geochemistry of trace elements in pyrites, it is possible to define that Juruena gold deposits is a magmatic-hydrothermal system, with hot CO_2-fluid rich that evolve to lower temperature, aqueous fluids. The gold was precipitated directly from the hydrothermal solution during different pulses. The formation processes of the Juruena gold deposit are most similar with a typical small Au-porphyry system formed in the Paleoproterozoic.

Introduction

THE JURUENA GOLD DEPOSIT is located on the western sector of the Alta Floresta Gold Province (AFGP), southern portion of the Amazonian Craton (Brazil; Fig.1). This province extends over 500 km NW-SE and historically has been an important gold-producing region (5.3 million ounces of gold between 1980 and 1999; Paes de Barros, 2007). The majority of gold deposits are concetrated and exploited by artisanal prospects. Due to its complexity, these deposits are not clearly classified.

Previous studies developed in the eastern sector of the AFGP have focused on geochemistry, hydrothermal alteration (Souza et al., 2005; Paes de Barros, 2007; Silva and Abram, 2008; Assis, 2011), structural controls on gold mineralization (Miguel Jr, 2011), and determining the evolution of mineralizing fluids (Moura et al., 2006). The Juruena gold deposit is a very good example of gold mineralization related with plutono-volcanic sequences within the AFGP, providing a good opportunity to document one of the most important gold deposit in the western part of the province.

The aim of this study is to determine the history and evolution of the ore formation in the Juruena gold deposit. We present a description of the vein paragenesis, stable isotopes, fluid inclusions and trace element geochemistry (EPMA) from main mineralized veins. Also we defined the absolute timing of the intrusive and the mineralization, using two different methods: U-Pb dating of zircon from the granitic rocks to constrain the age of magmatism and Re-Os dating of molybdenite to obtain the age of the gold mineralization event.

Regional Geology

The Alta Floresta Gold province (AFGP) is located between the limits of two geochronological provinces (Fig. 1; Santos et al., 2000), Tapajós-Parima (2.03 Ga to 1.88 Ga) and Rondônia-Juruena (1.82 Ga to 1.54 Ga). The AFGP is formed primarily by plutono-volcanic sequences generated in continental arc settings during the Paleoproterozoic (Fig. 2), containing different gold mineral deposits, all of this hosted in granitic rocks and occasionally in volcaniclastic sequences.

Souza et al. (2005) proposed that the province was formed during the development of the Juruena Magmatic Arc (1.85 – 1.76 Ga; Rondônia-Juruena Province), accreted to Tapajós-Parima Province (2.03 to 1.88 Ga). In the AFGP the Tapajós-Parima province is comprised by a post-collisional granitic magmatism defined by the Matupá Intrusive Suite (1872 ± 12 Ma; Fig.2) and by the basic rocks, generated in a continental setting from Flor da Serra Intrusive Suite (1879 ± 15 Ma; Fig.2).

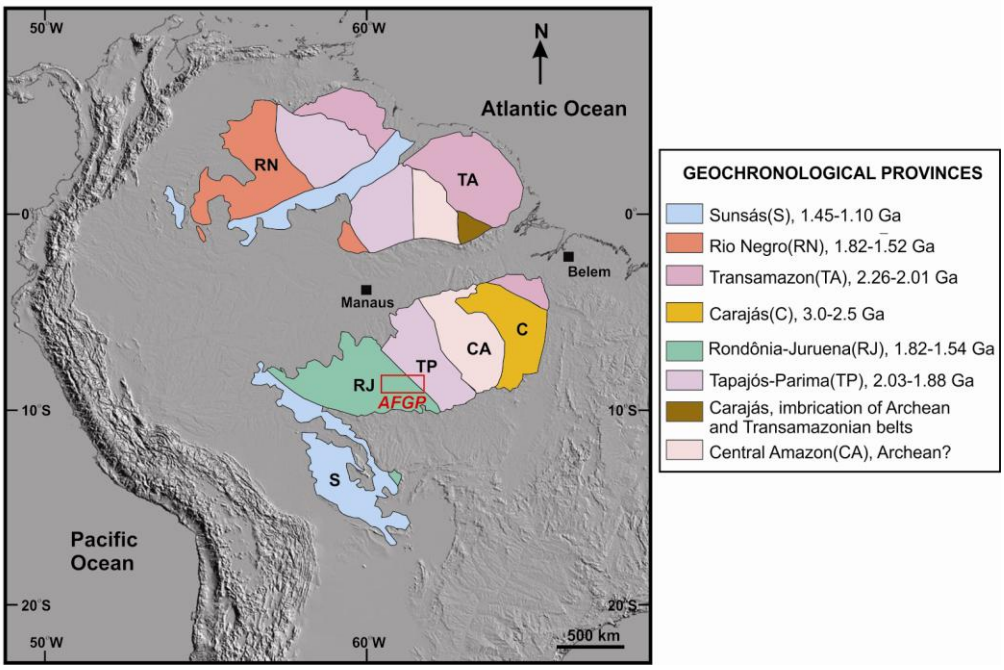

Figure 1. Geological map of the Amazon Craton showing the Geochronological Provinces and the location of the Alta Floresta Gold Province (AFGP) (modified from Santos et al., 2000)

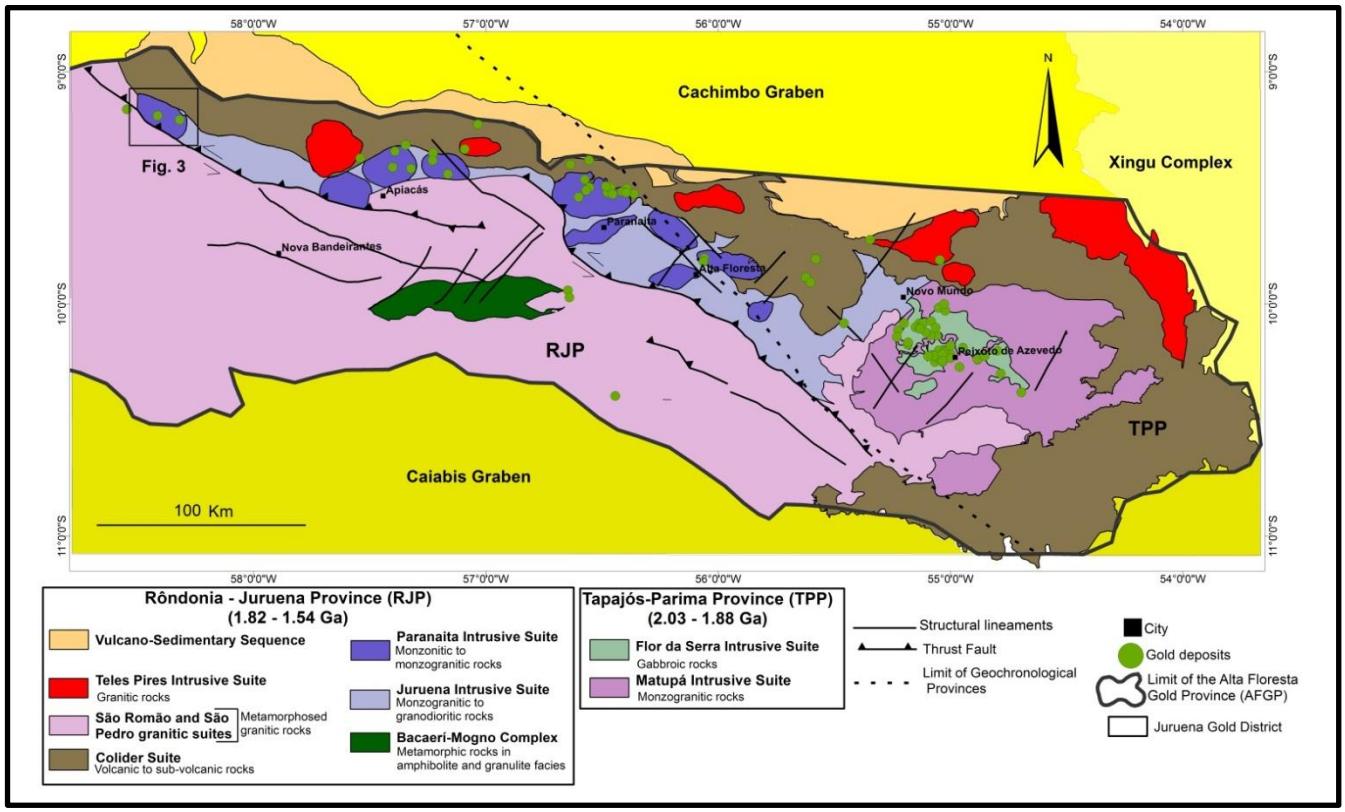

Figure 2. Regional map of the Alta Floresta Gold Province (AFGP), showing the approximate limit between Tapajós– Parima and Rôndonia-Juruena geochronological provinces according to Duarte et al. (2012). Location of Juruena gold deposit is showed in the left square of the figure (modified from Souza et al., 2005).

The convergent orogenesis that shaped the Juruena Magmatic Arc (JMA) started in about 1820 Ma ago. Compressive movements from SW to NE displaced an oceanic crust (Bacaerí-Mogno Complex) in the direction of the already cratonized Tapajós Magmatic Arc, resulting in plate subduction and comsuption (Duarte et al., 2012).

In the Juruena magmatic arc the basement rock is comprised by the Bacaerí-Mogno Complex (undated), that contain several remains of an oceanic crust associated with terrigenus material represented by amphibolite and granulite facies metamorphic rocks (Fig. 2). The basement is overlain by plutono-volcanic sequences (Fig.2): Juruena Intrusive Suite (1848 to 1823 Ma), Paranaíta Intrusive Suite (1819 to 1793 Ma), and Colíder Suite (1786 to 1781 Ma), (Fig. 2; Souza et al., 2005; Santos et al., 2008). Metagranites unites are also present, including São Romão Granite (1770 Ma) and São Pedro Granite (1784 Ma). Post-colissional granites intruded these rocks and have been assigned to Teles Pires Intrusive Suite (1756 ± 16 Ma). Beneficiente group (1700 – 1400 Ma) and Dardanelos Formation (~1400 Ma), volcano-sedimentary units, complete the stratigraphy of the extensional period (Fig. 2).

The great majority of the gold deposits in the AFGP are hosted in relatively oxidized I-type, metaluminous to slightly peraluminous granitics rocks (tonalite – granodiorite to syenogranite) and more subordinately in volcanic/volcanoclastic sequences (Paes de Barros, 2007; Assis, 2011). Based on mode of ocurrences, ore mineral association and chemical signature the mineralization can be divided into two groups,: (1) Disseminated (e.g., Serrinha, Luizão, X1 and Pe Quente deposits) and (2) Structurally-controlled vein type (e.g., Paraíba and Buriti deposits).

Several WNW-trending sinistral strike-slip faults have been defined in the province, generated during a brittle-ductil regime (Souza et al., 2005). Gold mineralization is related to E-W and N-S trending structures (Miguel-Jr, 2012).

Geology of the Juruena Gold Deposit

The Juruena gold deposit has been worked since 1980s decade, where the majority of the gold deposits are concentrated and exploited by artisanal prospectors (garimpeiros). Is estimated that 450.000 ounces of gold have been produced from 1980 to 2000. Lago Dourado Minerals Ltd. acquired the property in 2010, starting an exploration work, defining very prospective areas, such as Crente (10.5m @ 14.6 g/t gold, 3.7m @ 131.3 g/t gold) and Uiliam (5.8m @ 52.4 g/t gold).

The Juruena gold deposit is spatially and temporally associated with felsic intrusions that were emplaced during multiples pulses of magmatism (Fig. 3). The present study is focused on the Uiliam and Crente targets (Fig.3).

Based in the previous geological information developed by the Brazilian Geological Survey (Companhia de Pesquisa de Recurso MInerais- CPRM; Souza et al., 2005), the Juruena deposit is hosted in the granitic rocks of the Paranaíta Intrusive Suite (1819 – 1793 Ma), previously defined by Oliveira & Albuquerque (2013), and Souza et al. (2005), as a unit formed by porphyrytic to equigranular monzogranite with biotite and hornblend as principal accessory minerals. The Paranaita intrusive suite has been classified as relatively oxidized I-type, calc-alkaline, high potassium, metaluminous to peraluminous, granitic rocks forming in continental arc; this rocks have mantle-derived magma affinities, together with calc-alkaline magmas with crustal contamination (collisional type magmatism; Ribeiro and Duarte, 2010; Duarte et al., 2012).

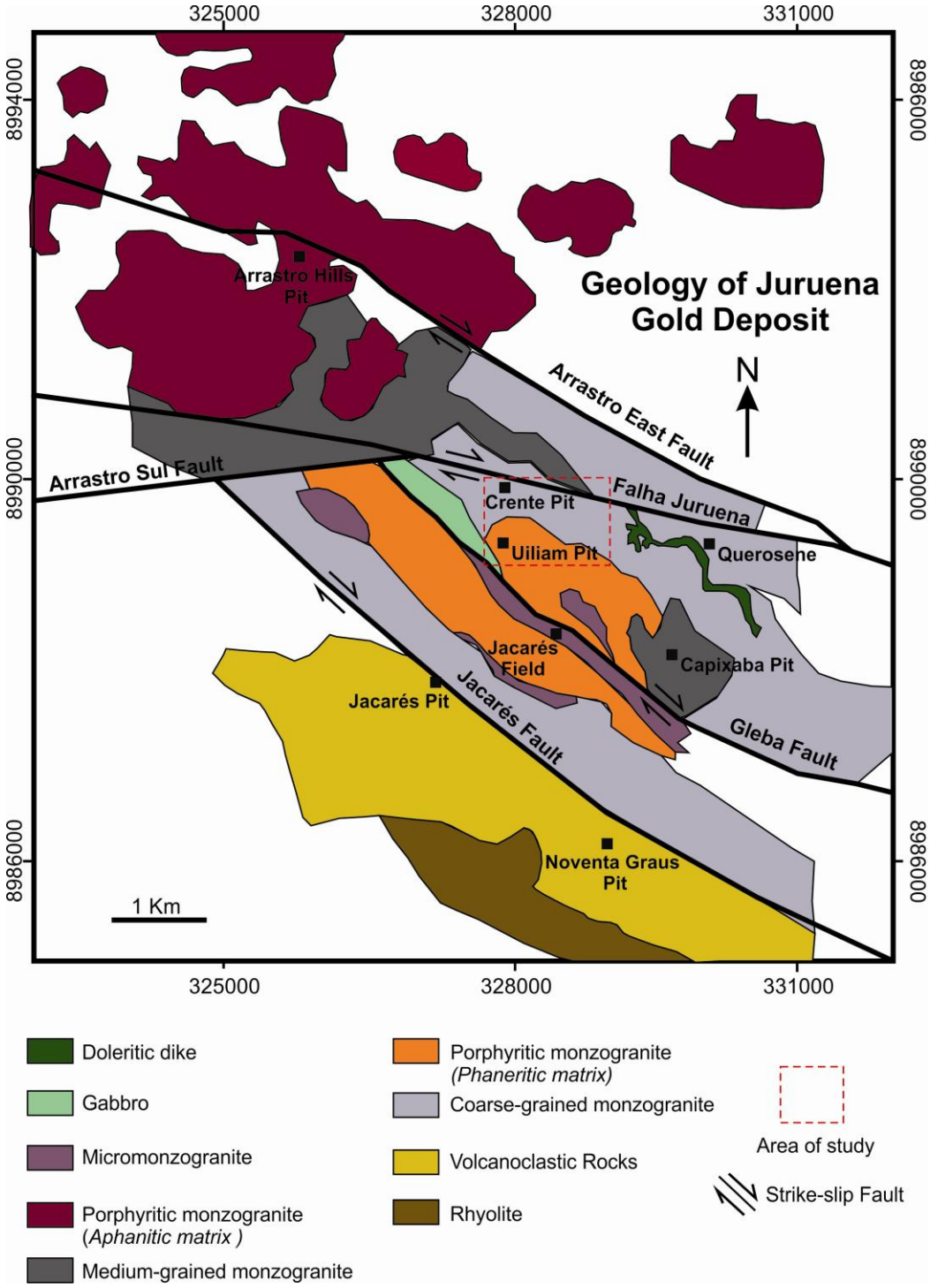

Figure 3. Generalized geological map of the Juruena gold area (modified from Lago Dourado Ltda, writ commun. 2011). Red square shows the studied targets in this work.

The dominant host rocks in the deposit are porphyritic to equigranular, medium to coarse-grained, biotite monzogranites (Fig. 4A-B), composed of K-feldspar (25–35%), plagioclase (30–40%), quartz (15–25%) and biotite (5–10%). Accessory minerals are hornblende, zircon, apatite, magnetite, rutile, titanite and ilmenite. These rocks are intruded by a micromonzogranite (Fig. 4C). All the sequence is crosscut by doleritic dikes (Fig. 4D).

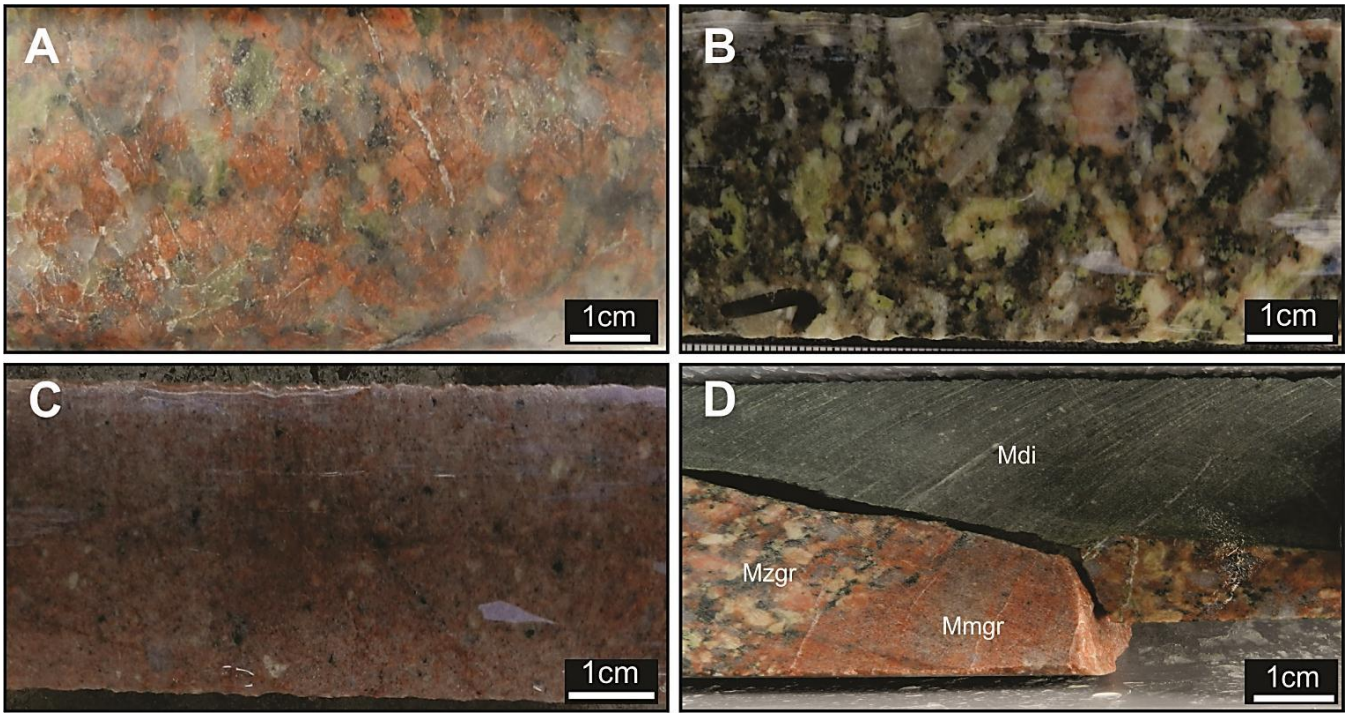

Figure 4. Hand specimen of altered host rocks in the Juruena gold deposit. (A) Biotite-monzogranite with intensive k-silicate alteration. (B) Porphyritic monzogranite with biotite. (C) Micromonzogranite with K-silicate alteration overprinted by a weak sericitic alteration. (D) Maffic dike in sharp contact with K-altered monzogranite and micromonzogranite. Abbreviations: Mzgr = Monzogranite, Mmgr = Micromonzogranite, Mdi= Maffic dike.

Several structural WNW striking faults have been identified in the Juruena area, some of which are controlling the gold mineralization. The WNW-ESE trending Juruena fault (Fig. 3) has been interpreted to be a principal structure, responsible of channelized some of the mineralizing fluids (Groves, writ commun., 2011). Other main structures include the Jacaré Fault, the Gleba fault and the Arrastro East fault (Fig. 3). These structures are parallel to the regional trends recognized for the AFGP.

Pyrite Textures

From the petrographical studies, four main types of hydrothermal pyrites have been recognized: pyrite 1 (py1) to pyrite 4 (py4), based on the interpreted paragenesis and the textures developed after acid etching. All the pyrites described below are in the quartz and calcite veins that represent the different stages in the deposit (Fig. 6). In the veins is possible to find two or more paragenetic types of pyrite.

Py_1 occurs euhedral to subhedral crystals, varying from 0.1 to 1 mm in size, containing abundant pores distributed homogeneously though the grain (Fig. 5A-B). In this type of pyrite inclusions of other minerals are uncommon. Rounded to subhedral py2 grains vary from 0.5 to 3mm in size, these type of pyrites are resistant to nitric acid etching (Fig. 5B). Py2 with no, or few, pores, is strongly fractured and it is crosscut py1. Py3 occurs as very porous, isolated anhedral crystals that vary from 0.5 to 2mm across (Fig. 5C), it contains inclusions of quartz. The last type of pyrite (py4), is compact and rounded (Fig. 5E), crystals varying from 0.2 to 2mm. The etching in this type of pyrite exposes an py4 with a porous core py_3 (Fig. 5F).

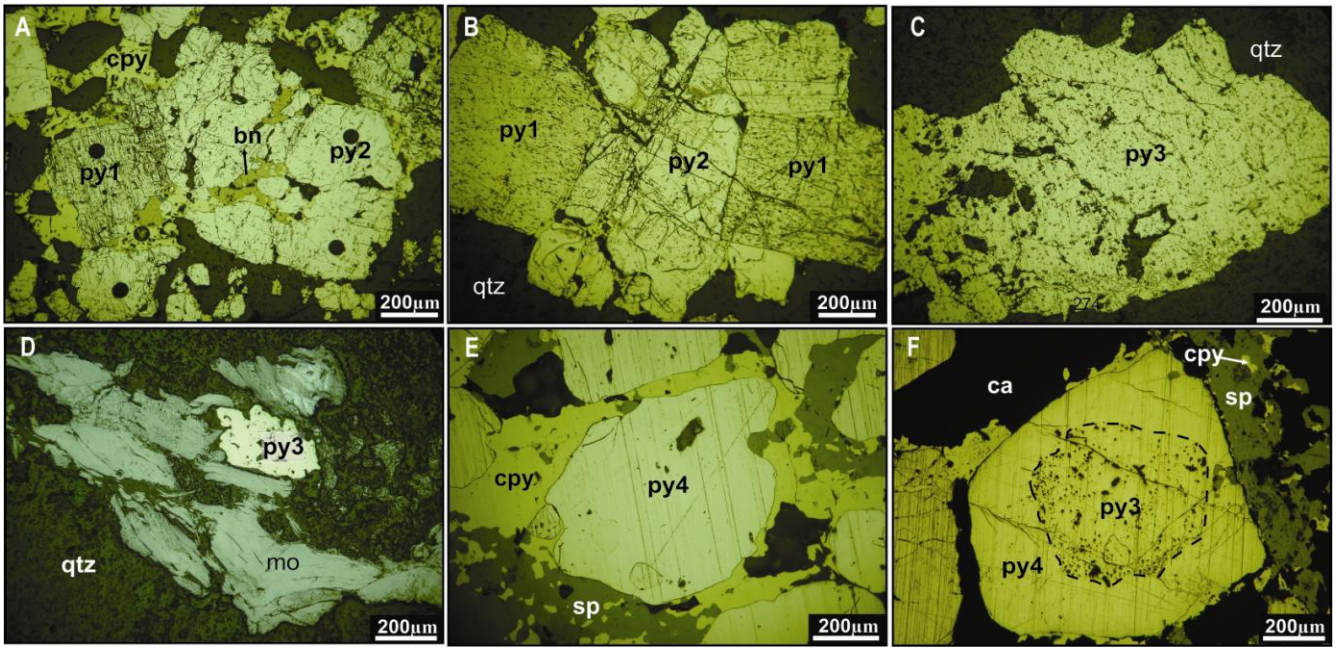

Figure 5. Photomicrographs of mineral assemblage and textures of pyrites in the Juruena gold deposit. Plane-polarized reflected light (A) chalcopyrite-pyrite-bornite in quartz vein in stage 1, py is present as py1 and py2. (B) Cluster of euhedral py1 crystal crosscut by subhedral py2 in stage 1.1. (C) Porous anhedral py3 with randomly oriented inclusions of silicate mineral (black), within a vein of quartz. (D) Molybdenite-pyrite in quartz vein with K-feldspar envelope. (E) Coarse-grained pyrite, chalcopyrite and sphalerite in calcite vein in stage 3. (F) Euhedral, non porous py_4 with core of py_3 with inclusions of silicate minerals (black). Abbreviations: py= pyrite, cpy= chalcopyrite, bn= bornite, sp= sphalerite, mo= molybdenite, Au= native gold, qtz= quartz, ca= calcite

Hydrothermal Alteration, Veins and Gold Mineralization

The host rocks in the Juruena gold deposit have been strongly altered. Hydrothermal alteration and mineralization assemblages have been divided into five stages. Also were defined several substages based on the classification of the individual veins related to a specific hydrothermal alteration (Fig. 6; Table 1). Stage 1 is characterized by K-silicate alteration and two generations of veining (substages 1.1 and 1.2). Stage 2 caused sericitic alteration, two types of veins were developed in this stage (substages 2.1 and 2.2). Carbonatization is the hydrothermal alteration in the stage 3. Silicification overprinted previous alteration in the stage 4. The final stage of the hydrothermal activity (Stage 5) produced propylitic alteration. The gold in the Juruena deposit is focused in the stage 1.1 and stage 3 (see below).

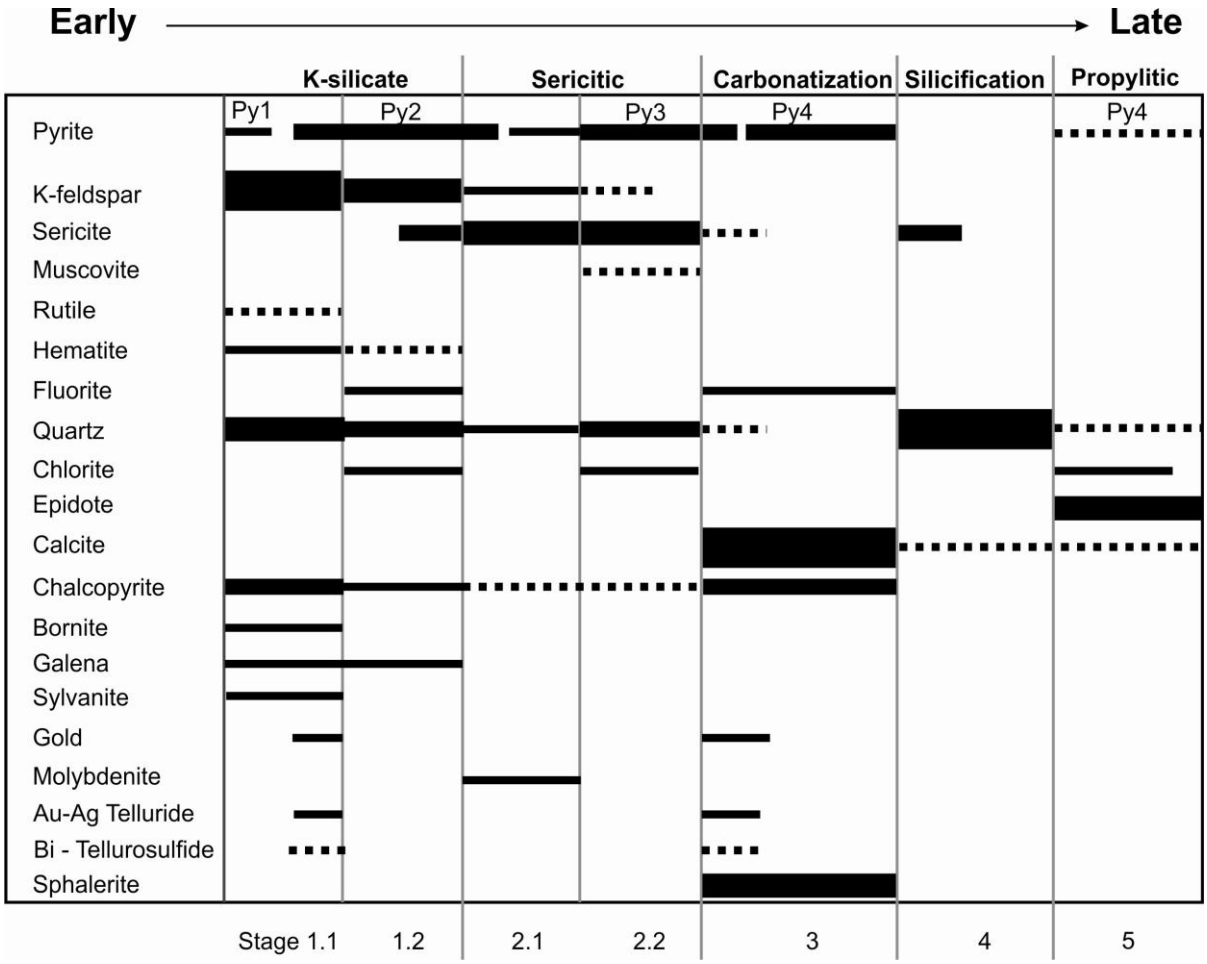

Figure 6. Paragenesis of the Juruena gold deposit.

Stage (Hydrothermal alteration)	Substage	Diagnostic Features	Accessory minerals	Vein morphology	Predominant Host rock
Stage 1 (Potassic)	1.1	Qtz + cpy + bn ± py and gold veins	Syl+ bi + ga + he + rutile.	Irregular	Biotite monzogranite
	1.2	Qtz + chl + fl ± py ± cpy veins	He		
Stage 2 (Sericitic)	2.1	Qtz + mo ± py veins with K-feldspar alt halos	Ms+ he + cpy	Irregular	Porphyritic monzogranite
	2.2	Qtz + ca ± py ± cpy +chl veins with ser halo	Ms + ga + he	Straight	
Stage 3 (Carbonatization)		Pervassive ca + sp + cpy + fl ± py and gold veins	Bi + Syl	Straight	Porphyritic monzogranite
Stage 4 (Silicification)		Pervassive and veins	Ca	Straight	Micromonzogranite, occasionally the others host rocks
Stage 5 (Propylitic)		Ep + chl ± ca ± qtz and ca, ep veins	Py ±cpy	Straight	Doleritic dikes

Table 1. Sequence of veins and gold mineralization at the Juruena deposit

Abbreviations: Qtz = quartz, cpy = chalcopyrite, bn = bornite, py = pyrite, syl = sylvanite, bi = biotite, ga = galena, he = hematite, chl = chlorite, fl = fluorite, mo = molybdenite, Ms = muscovite, ca = calcite, ser = sericite, ep = epidote.

Stage 1

This stage is well exposed in all the host rocks of the Juruena deposit. It is pervasive and characterized by the development of K-silicate that gives, a reddish appearance to the rock (Fig. 7A).

This event was a result of the alteration of the primary plagioclase and K-feldspar (Fig. 8A). Two parallel sets of veins associated with this stage have been divided into two substages, based on mineral assemblage composition.

In substage 1.1, quartz-sulfides veins are associated with the intensively K-silicate alteration (Fig. 9A), chalcopyrite and pyrite (py1 and py2; Fig. 5B) are the main sulfide minerals and occurs with accessory bornite, galena, and tellurides. Quartz-chlorite-fluorite-pyrite (py2) veins (Fig. 9B) formed the substage 1.2, parallel to substage 1.1. This substage is unmineralized and the presence of interstitial hematite is very common.

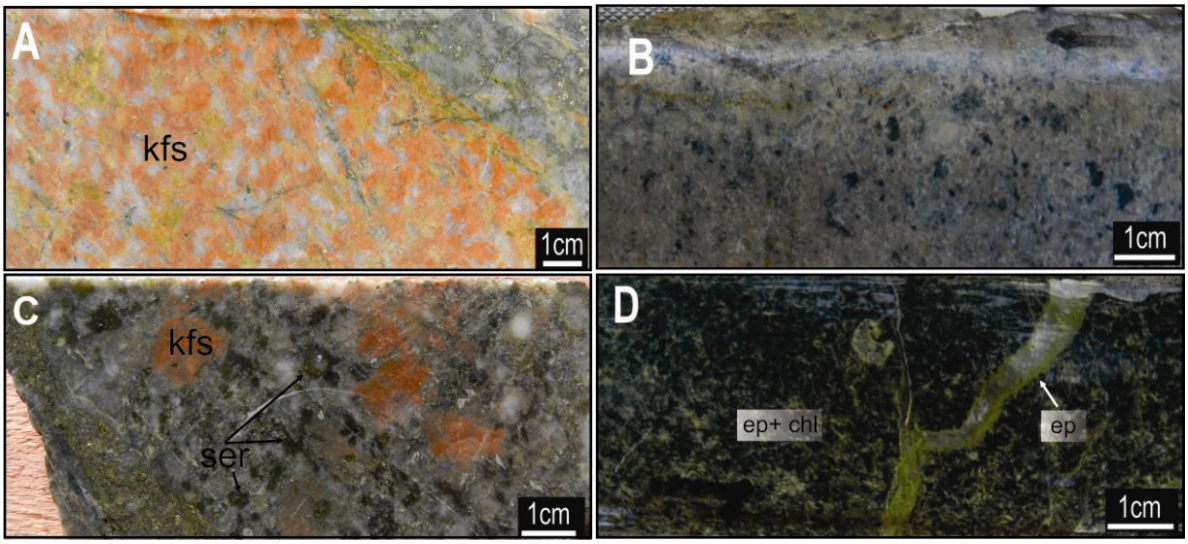

Figure 7. Hand specimen of hydrothermal alteration.(A) Intensive K-silicate alteration.(B) Pervassive sericitic alteration in the porphyritic monzogranite (C) Sericitic alteration overpinting K-silicate alteration. (D) Doleritic dike strongly affected by propylitic alteration with epiode-calcite-chlorite. Abbreviations: kfs= k-feldspar, ser= sericite, ep = epidote, chl= chlorite

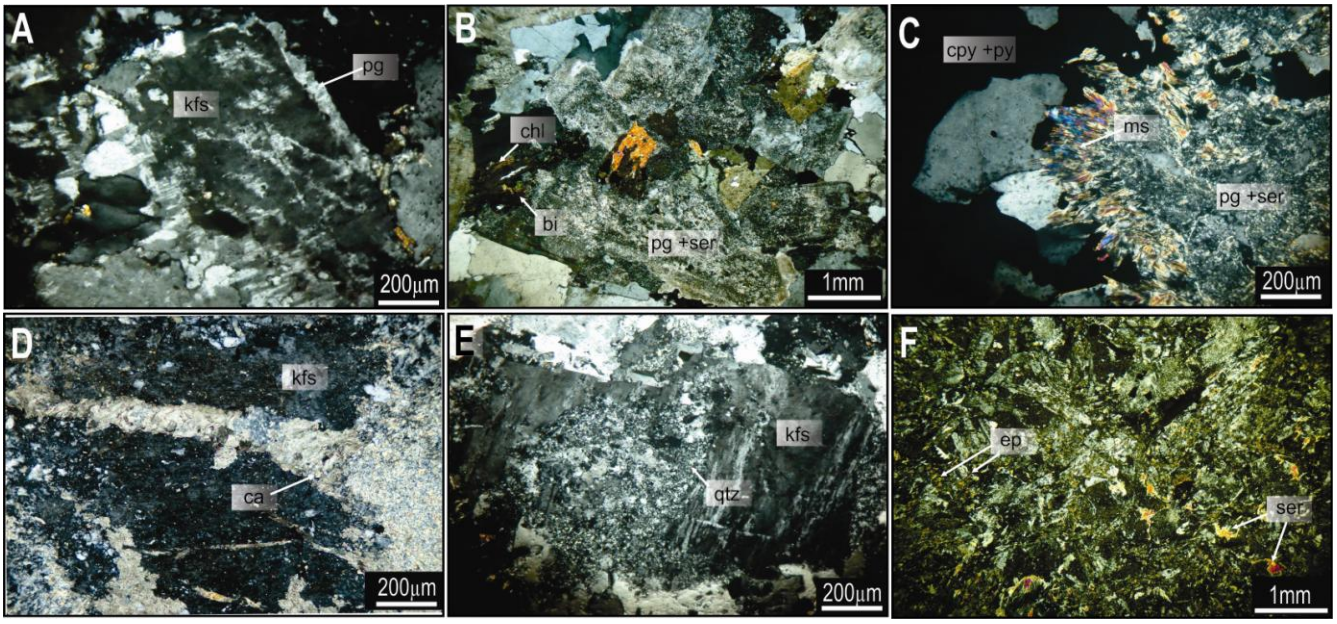

Figure 8. Hydrothermal alteration assemblage (cross-polarized transmitted light). (A) K- silicate alteration with K feldspar replacing plagioclase from monzogranite. (B) Plagioclase and biotite from the monzogranite replaced by sericite and chlorite, respectively. (C) Zone with strong sericitic alteration developing muscovite. (D) Carbonatization overprints all the previous alteration types. (E) Silicification: quartz reeplacing K-feldspar from the monzogranite. (F) Propylitic alteration in doleritic dike. Abbreviations: kfs= k-feldspar, ser= sericite, ep= epidote, pg= plagioclase, bi= biotite, chl= chlorite, ms= muscovite, ca= clacite, py= pyrite, cpy= chalcopyrite.

Stage 2

This stage is characterized by the pervasive sericitic alteration (Fig. 7B), that overprinted the previous K-silicate alteration (Fig. 7C). Stage 2 is typified by the quartz-sericite-chlorite-pyrite (py_3) assemblage. Plagioclase is almost completely altered to sericite and the biotite to chlorite (Fig. 8B). In the places where the hydrothermal alteration is very strong, muscovite is developed (Fig. 8C). Two

individual vein assemblages have been differentiated (Fig. 6; Table 1): substage 2.1 with milky quartz and, as most import sulfides, molybdenite and pyrite (py_3; Fig. 5C-D). These veins have a halo of fine-grained granular K-feldspar (Fig. 9C). Substage 2.2 consists of quartz-pyrite (Py3) veins with a sericite-chlorite halo (Fig. 9D), and chalcopyrite as accessory mineral. Both stages are parallel and were not possible to identify any crosscutting relationships.

Stage 3

Stage 3 is the second high-grade gold mineralizing event, and is associated with the development of disseminated calcite (Fig. 8D) and calcite-sulfide veins filling fractures

generated by previous processes (Fig. 9E). The main sulfides are sphalerite-chalcopyrite-pyrite (py_3 and py_4; Fig. 5E). Internal textures in the pyrites are very typical in this stage (Fig. 5F).

Stage 4

This stage is defined by an intensive silicification process, filling fractures and replacing all the previous hydrothermal minerals (Fig. 8E). Different veins were developed in this stage but all of them are unmineralized.

Stage 5

The last hydrothermal stage is restricted to latest doleritic dikes (Fig. 7D). This rocks are strongly altered with propylitic alteration formed by fine-grained epidote-chlorite-calcite replacing the previous igneous minerals (Fig. 8F). Veins of calcite and epidote cut this intensively altered rock. Stage 5 contains only minor unmineralized pyrite.

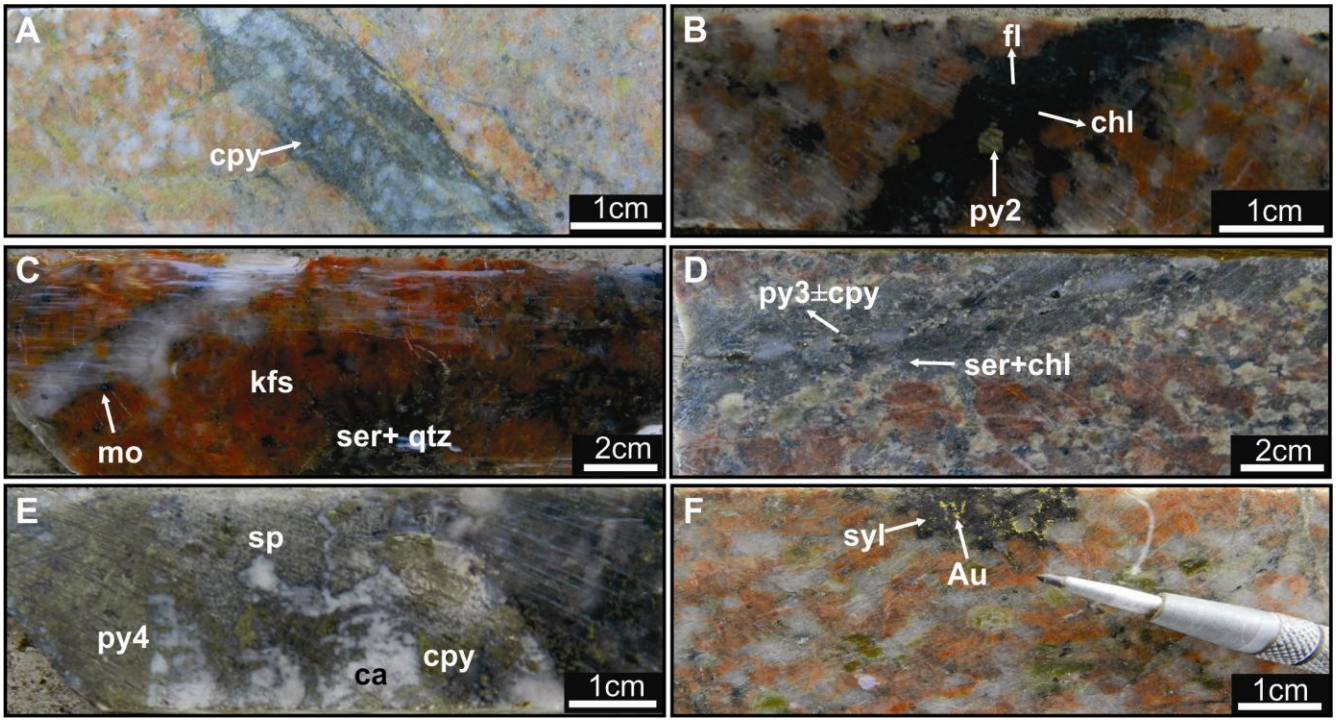

Figure 9. Mineralized veins in hand specimen at the Juruena gold deposit. (A) Stage 1.1 vein of qtz-cpy-py in K-silicate alteration. (B) Stage 1.2 vein of quartz-chlorite-pritey-fluorite. (C) Stage 2.1 vein of quartz-molybdenite-pyrite within a K-feldspar envelope into the porphyritic monzogranite with a pervasive sericitic alteration. (D) Stage 2.2 vein of quartz-pyrite with sericite-chlorite envelope crosscut the porphyritic monzogranite, sericitic alteration overprinting the previous K-silicate alteration. (E) Stage 3 vein of calcite–sphalerite-chalcopyrite-pyrite, this event is overprinting the previous alterations. (F) Free gold in paragenesis with Au-Ag Tellurides (Sylvanite) in stage 1.1. Abbreviations: qtz = quartz, py= pyrite, cpy= chalcopyrite, fl= fluorite, chl= chlorite, mo= molybdenite, ser= sericite, sp= sphalerite, Au = gold, Syl = sylvanite, kfs = k-feldspar

Gold mineralization was evident in the substage 1.1 and stage 3 associated with veins. In substage 1.1, gold appears as small inclusions in the pyrite (Fig. 10A) and filling spaces between different pyrite generations (Fig. 10B). Occasionally, in this same stage, is possible to find clots of free gold in paragenesis with gold-silver tellurides (sylvanite?; Fig. 9F, 10C). In stage 3 Gold is presents as small inclusions in pyrite and chalcopyrite crystals (Fig. 10D).

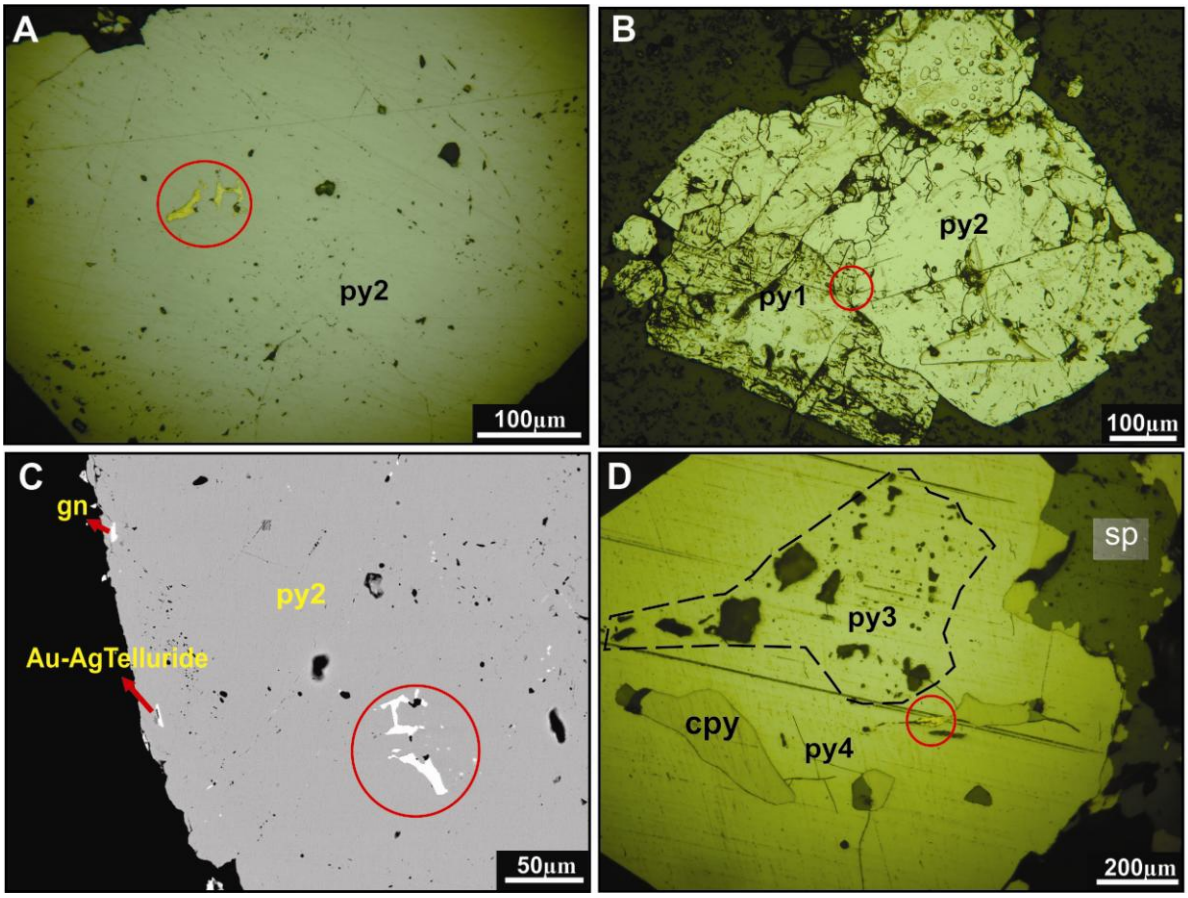

Figure 10 Photomicrographs (A-C) and back-scattered image (D) of the high grade mineralization at Juruena gold deposit. (A) Native gold as small inclusions in py2. (B) Gold filling the contact between two different py generations. (C) Free gold (red circle), micro-size particles of Ag-Au Telluride (Sylvanite?) and galena all of them in py2. (D) Py4 with core of py3 containing inclusions of native gold and silicate (black). Abbreviations: py= pyrite, cpy = chalcopyrite, gn = galena, sp =sphalerite.

Analytical Methods

U-Pb Geochronology

Samples of two monzogranitic rocks were selected for the Sensitive High Resolution Ion Microprobe (SHRIMP IIe) zircon geochronology, in order to constrain the timing of crosscutting relationships defined in the field work. Sample 21 was collected from the biotite monzogranite, principal host rock of the gold mineralization (Fig. 4A), whereas sample 25 was from the micromonzogranite that crosscuts the biotite monzogranite (Fig. 4C-D).

U- Th- Pb analysis in zircon were executed using Sensitive High Resolution Ion Microprobe (SHRIMP IIe) at the Geochronology Center, University of São Paulo. Details of the analytical procedures using SHRIMP have been described by Williams (1998) and Deng et al., (2012).

In the SHRIMP analyses, the ion current was 2.5-4.5nA and the spot size averaged 25 μm, using a peak jumping scanning mode. The standard zircons used were the TEMORA 2 (417 Ma; $^{206}Pb/^{238}U$=0.066683; Black et al., 2003). The standard sample was measured after every four points, in order to certify the reliability of the measurements and the operation of the instrument. The data was processed using ISOPLOT 4 program (Ludwig, 2003). The age uncertainties are presented as 1σ. Weighted average ages of $^{206}Pb/^{238}U$ used a confidence level of (1σ) 95%. The results are listed in Table 2.

Re-Os Geochronology

One molybdenite sample, coexisting with gold-richest pyrite (py3) in substage 2.1, was analized in order to determine the age of mineralization. The sample was collected from drill hole JRND-059, Uiliam area. Re–Os isotope analyses were carried out at the Radiogenic Isotope Facility of the Department of Earth and Atmospheric Sciences, University of Alberta, Canada.

Concentrates of molybdenite were obtained using different mineral separation techniques as Frantz isodynamic magnetic separator in combination with heavy liquids. Final molybdenite concentrates were hand-picked under miscrocope. Sample was equilibrated using Carius tubes (Selby and Creaser, 2003). The chemical separation and purification of Re and Os follows the protocols defined by Azmy et al., (2008). Purified Re and Os concentrates were loaded onto Ni and Pt filaments and the Re and Os concentrations and isotopic composition were measured using isotope dilution-negative thermal ionization mass spectrometry (ID-TIMS; Creaser et al., 1991) on a Micromass Sector 54 spectrometer. Re-Os model age error is reported at 2σ and all the values were normalized using a Re-Os decay constant of Smoliar et al., (1996).

Microthermometry

A total of 4 doubly polished thin sections from the principal veins were prepared in order to compare fluid temperature and composition. Microthermometry analysis were conducted on a Linkam THSM600 microthermometric stage at the University of Campinas. Fluid inclusions were cooled until -120 ^{o}C and heated progressively until total homogenization. Calibration was carried out at the beginning and end of the study using CO_2 and H_2O synthetic fluid inclusions. The precision for freezing runs is about ± 0.1 ^{o}C and for heating runs ± 2 ^{o}C.

Salinities are reported based on the final ice melting for halite-undersaturated inclusions (Bodnar, 1993) and CO_2-clathrate (Collins, 1979). In the petrography was defined halite-bearing fluid inclusions, in this case the salinities were calculated using the dissolution temperatures of the daughter mineral (Sterner et al., 1988).

Stable Isotopes

Analyses of oxygen and sulfur isotopes were carried out at the United State Geological Survey (USGS) stable isotope facilities in Denver, Colorado.

Sulfur Isotopes: Sulfide minerals were analyzed for sulfur isotopes. For this, clean hand-picked samples were selected. Mineral samples that included pyrite and chalcopyrite were combusted and analyzed for $\delta^{34}S$ according to methods purposed by Giesemann et al., (1994). Sulfide powders were weighed into the tin capsules with vanadium pentoxide, and the analysis were carried out using a CE Elantech Inc. Flash 2000 Elemental Analyzer coupled to a ThermoFinnigan Delta Plus XP ™ continuous flow mass spectrometer. All sulfide samples were analyzed alongside nationally accepted standards NBS123+17.44 per mil and IAEA-S-3 -32.55 ± 0.12 per mil (Coplen et al., 2002). Isotopic compositions are reported in δ-notation relative to Vienna Cañon Diablo Troilite (V-CDT) with a reproducibility of 0.3‰. Duplicate analysis agreed to within ± 0.5‰.

Oxygen Isotopes*:* Clean, hand-picked samples of silicates were analyzed for oxygen isotopes. The analytical method used closely follows the procedures described by Clayton and Mayeda (1963), using BrF_5. Mineral separates were reacted with BrF_5 to produce oxygen which was in turn reacted with carbon. The resulting CO_2 gases were measured using the Finnegan-MAT 252 mass spectrometer. Results are expressed in δ-notation relative to V-SMOV (standard mean ocean water) with a reproducibility of 0.3‰; duplicate analyses generally agree to within ±0.3‰.

Geochemistry of the pyrite- Electron Probe Microanalysis (EPMA)

Spots in all type of pyrites were obtained using a JEOL JXA-8900 microprobe with five wavelength dispersive spectrometers at the USGS in Denver, Colorado. The operating conditions were: 15 Kv and 10 nA of probe current. The electron beam was ~5 μm in diameter. A set of native elements and sulfides, including Te, Sb, Au, As, Cu, TlBr and FeS were used as reference materials. Analyzed elements included Cu, Fe, As, S, Sb, Te, Au, Tl and Cl.

Results

U-Pb geochronology

Most of the separated zircon grains from both type granitic rocks were transparent or partly translucent, euhedral to subhedral, with prism shapes and without core-rim structures or cracks.

Table 2. SHRIMP zircon U/Pb analytical data from granitic host rocks of the Juruena gold deposit.

Spot	U (ppm)	Th (ppm)	$^{232}Th/^{238}U$	Pb (%)	Pb (ppm)	Isotopes ratios(1σ)			Ages (Ma, 1σ)	
						$^{207}Pb/^{206}Pb$	$^{207}Pb/^{235}U$	$^{206}Pb/^{238}U$	$^{206}Pb/^{238}U$	$^{207}Pb/^{206}Pb$
Sample 21										
21-1.1	514	153	0.31	0.00	82.0	0,103 ± 0.9	2,64 ±2.1	0,186 ± 1.9	1097 ± 19	1680 ± 16
21-2.1	108	129	1.23	0.25	26.4	0,110 ± 1.6	4,27 ± 2.6	0,283 ± 2.0	1607 ± 29	1791 ± 29
21-3.1	238	217	0.94	0.04	63.9	0,111 ± 0.9	4,79 ± 2.1	0,313 ± 1.9	1755 ± 29	1817 ± 17
21-4.1	182	270	1.53	0.11	49.8	0,111 ± 1.1	4,85 ± 2.3	0,318 ± 2.0	1778 ± 30	1812 ± 20
21-5.1	211	167	0.82	0.00	51.4	0,109 ± 1.0	4,26 ± 2.3	0,284 ± 2.0	1610 ± 29	1780 ± 19
21-6.1	124	91	0.75	0.09	34.0	0,112 ± 1.3	4,91 ± 2.3	0,318 ± 2.0	1782 ± 31	1830 ± 23
21-7.1	168	134	0.83	4.14	48.6	0,109 ± 5.7	4,80 ± 6.5	0,321 ± 2.0	1794 ± 32	1776 ± 113
21-8.1	185	179	1.00	0.07	48.3	0,110 ± 1.1	4,58 ± 2.2	0,303 ± 1.9	1706 ± 29	1792 ± 21
21-9.1	152	142	0.96	0.00	41.4	0,111 ± 1.1	4,85 ± 2.2	0,317 ± 1.9	1774 ± 30	1816 ± 20
21-10.1	326	198	0.63	0.04	53.2	0,110 ± 1.0	2,89 ± 2.1	0,190 ± 1.9	1122 ± 19	1802 ± 18
21-11.1	315	212	0.69	0.39	85.3	0,101 ± 1.2	4,76 ± 2.2	0,314 ± 1.9	1760 ± 29	1798 ± 21
21-12.1	227	252	1.15	0.26	59.4	0,111 ± 1.2	4,64 ± 2.3	0,304 ± 1.9	1710 ± 28	1813 ± 22
21-13.1	158	115	0.75	0.19	40.8	0,109 ± 1.3	4,50 ± 2.4	0,300 ± 1.9	1691 ± 29	1781 ± 25
21-14.1	205	160	0.81	0.23	56.0	0,108 ± 1.2	4,72 ± 2.3	0,317 ± 1.9	1776 ± 30	1763 ± 22
21-15.1	250	207	0.86	0.04	67.8	0,108 ± 0.9	4,73 ± 2.1	0,316 ± 1.9	1771 ± 29	1775 ± 16
Sample 25										
25-1.1	236	161	0.71	0.10	63.8	0,110 ± 1.0	4,76 ± 2.1	0,32 ± 1.9	1765 ± 29	1792 ± 18
25-2.1	156	152	1.00	0.08	43.3	0,110 ± 1.3	4,88 ± 2.3	0,32 ± 1.9	1800 ± 30	1799 ± 23
25-3.1	137	112	0.85	0.10	37.6	0,110 ± 1.2	4,85 ± 2.3	0,32 ± 2.0	1790 ± 31	1797 ± 23
25-4.1	121	110	0.93	0.23	32.8	0,110 ± 1.7	4,76 ± 2.6	0,31 ± 2.0	1760 ± 31	1798 ± 31
25-4.2	535	349	0.67	0.00	140.4	0,110 ± 0.6	4,64 ± 2.0	0,30 ± 1.9	1719 ± 29	1803 ± 11
25-5.1	152	182	1.23	0.03	41.5	0,110 ± 1.1	4,83 ± 2.2	0,32 ± 1.9	1775 ± 30	1807 ± 21
25-6.1	77	76	1.03	0.00	21.0	0,108 ± 1.7	4,77 ± 2.7	0,32 ± 2.1	1785 ± 32	1775 ± 31
25-7.1	183	152	0.86	0.00	53.4	0,111 ± 1.0	5,22 ± 2.2	0,34 ± 1.9	1882 ± 32	1826 ± 19
25-8.1	130	109	0.86	0.08	35.6	0,110 ± 1.3	4,86 ± 2.4	0,32 ± 2.0	1785 ± 31	1806 ± 24
25-9.1	62	48	0.79	0.00	17.6	0,111 ± 1.8	5,02 ± 2.8	0,33 ± 2.2	1830 ± 35	1815 ± 34
25-10.1	268	221	0.85	0.00	70.7	0,111 ± 0.9	4,69 ± 2.1	0,31 ± 1.9	1728 ± 29	1810 ± 16
25-11.1	110	83	0.78	0.44	29.3	0,107 ± 2.6	4,56 ± 3.3	0,31 ± 2.0	1737 ± 31	1748 ± 47
25-12.1	122	101	0.86	0.22	32.9	0,108 ± 1.4	4,65 ± 2.4	0,31 ± 2.0	1759 ± 31	1759 ± 25
25-13.1	127	104	0.85	0.08	35.5	0,111 ± 1.2	4,99 ± 2.5	0,33 ± 2.1	1820 ± 34	1816 ± 22
25-14.1	152	124	0.84	0.00	43.8	0,108 ± 1.4	5,00 ± 2.4	0,33 ± 2.0	1860 ± 32	1773 ± 26
25-15.1	306	345	1.17	0.07	85.6	0,109 ± 0.8	4,90 ± 2.1	0,32 ± 1.9	1816 ± 30	1787 ± 16
25-16.1	948	1818	1.980743	0.11	221.2	0,109 ± 0.5	4,08 ± 2.3	0,27 ± 2.2	1547 ± 30	1784 ± 10

Multiple oscillatory growths are frequently displayed by cathodoluminescence analyses, typically of magmatic zircons (Fig. 11A, C). Localities of SHRIMP measurement spots are positioned within the closed rhythmic rings (Fig. 11A, C). Zircon U-Pb analyses are present in two age groups: $^{206}Pb/^{238}U$ and $^{207}Pb/^{206}Pb$. The crystallization time of the pluton was determined on the basis of $^{206}Pb/^{238}U$ and present in the U/Pb concordia plot.

Biotite monzogranite (sample 21): Fifteen analyses in 15 grains of zircon were analyzed. Uranium content had a long variation in zircon grains (124ppm-514ppm). The ratio Th/U is between 0.71-1.98. Ages ranging from 1755 ± 29 to 1794 ± 32 Ma were yielded, excluding the spots 1.1 and 9.1 for the high concentration of U. Spots 1.2, 4.1, 7.1, 11.1 and 13.1 were also excluded because they were far from the concordant plot. The crystal 6.1 had a high anomaly in Pb and as, a consequence, has been left out to calculated the age (Table 2). The Concordia age calculated with seven spots is 1790±6.4 Ma (Fig. 11B).

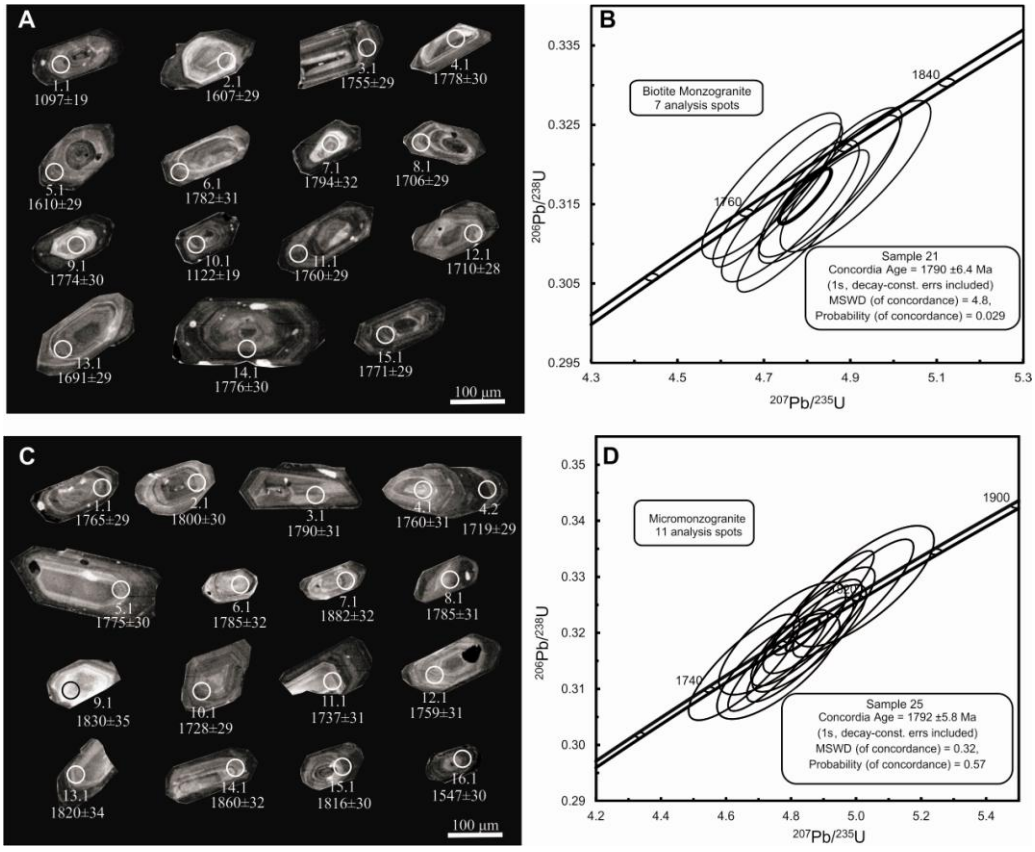

Figure 11. Cathodoluminescence images and location of SHRIMP spots measurements of zircon from monzogranite (A) and micromonzogranite (C), and U/Pb concordia diagram from same samples: monzogranite (B) and micromonzogranite (D).

Micromonzogranite (sample 25): Sixteen zircon grains were analyzed with 17 spots. The uranium content of zircons from this rock varies in the range of 62 ppm and 948 ppm. Of these analyses, only the measurement 16.1 gave a high Th/U ratio, which was greater than 1.98. Dating of eleven from the seventeen zircon grains show ages that cluster between 1759 ± 31 to 1830 ± 35 Ma. Spots 7.1 and 14.1 are older (1883 ± 32 and 1860 ± 32 Ma), it can be explained by the incorporation of oldest zircon crystal from an older magmatic event. Spots 4.2, 10.1 and 11.1 were younger (1719 ± 29, 1728 ± 29 and 173 ± 31 Ma). Both cases are far from de concordant plot. The ages of the eleven zircons were plotted on the concordia curve, and the age of this rock is calculated at 1792 ± 5.8 Ma (Fig. 11D).

Re-Os geochronology

Rhenium-Osmium dating was obtained in one sample of molybdenite from the stage 2.1, related with Au-bearing pyrite. Re content of the sample was 620 ppm and common Os was 3.0 ppb (Table 3). The detected Os is radiogenic. Re-Os model age of molybdenite is 1805 ± 7 Ma (Table 3).

Table 3. Re-Os Isotope result for molybdenite from Juruena Gold Deposit

Sample ID	Brief sample description	Re (ppm)	±	^{187}Re (ppm)	±	^{187}Os (ppb)	±	Common Os (ppb)[1]	Model age (Ma)[2]	± (Ma)
023	Quartz-molybdenite vein	620	1.6	389701	1008	11897	8	3	1805	7

Analytical uncertainties are reported at 2σ

[1]Ammount of common Os above analytical blank in ppb

[2]Model age calculated from the simplified equation [$t = \ln(^{187}Os/^{187}Re+1)/\lambda$ where t = model age and $\lambda = ^{187}$Re decay constant], assuming no initial radiogenic Os.

Sulfur Isotope

Results of thirteen analysis for sulfide minerals from the different stages in Juruena gold deposit are listed in Table 4. The $\delta^{34}S_{sulfide}$ values range between -7.8‰ and 1.5‰ for pyrite (*n*=7) and between -7.1‰ and -1.9‰ for chalcopyrite (*n=6).*

Sulfides from each stage display a short interval in isotopic composition, although the samples from substage 1.1 are isotopically lighter than in comparison of the samples from the other stages. The $\delta^{34}S$ values at Juruena deposit define a spatial zonation pattern, characterized by $\delta^{34}S$ depleted sulfides in the earliest stages (substage 1.1 and 1.2) and progressively enrichment in

$\delta^{34}S$ composition with distance from the mineralized zone, where the highest values appear (stage 3).

TABLE 4. Sulfur isotopic result for sulfide minerals from the Juruena gold deposit.

Sample ID	Mineral	Stage	$\delta^{34}S$ (‰)
40	cpy	1.1	-4.5
57	cpy	1.1	-6.8
57	py	1.1	-7.8
66	cpy	1.1	-7.1
43	cpy	1.2	-3.1
50	py	1.2	-3.1
50	cpy	1.2	-4.9
53	py	1.2	-3.2
70	py	2.2	0.3
77	py	2.2	-0.5
79	py	2.2	-4.0
26	py	3	1.5
26	cpy	3	-1.9

Abbreviation: cpy = chalcopyrite, py = pyrite.

Fluid Inclusions

Fluid inclusion analyses were focused on the base of fluid inclusions assemblage defined by Goldstein and Reynolds (1994), where a group of fluid inclusions were trapped synchronously along the primary structure in the minerals. At Juruena deposit, it is difficult to identify fluid inclusions in quartz that satisfy the above criteria, because multiple events mix the fluids and generate superposition during the evolution of the system. In the veins related with the early stages, quartz with growth texture are extremely rare. The majority of fluid inclusions occur in ramdon groups, without any evidence for contemporaneous trapping. All the fluid inclusions in this study occur in groups that contain similar number and volume proportion of phases defined in the petrographical studies. We assume that the groups of inclusions that have similar heating and freezing temperatures were originated form a similar fluid under similar conditions. Samples in this study were mainly from quartz formed in stages 1 and 2.

Based on the phases present at room temperature, four types of fluid inclusions were distinguished and classified according to the classification of Rusk et al. (2008), as type B20, B20H, C50 and B15. In this classification sytem, the letter “B” denotes “bubble,” and the number indicates the average volume percent occupied by the bubble (vapor) in the different type of inclusions. The letter “H” refers to halite as daughther mineral and letter “C” represents the

inclusions that contain a carbonic gas (CO_2-rich) and immiscible aqueos liquid. In all the cases the fluid inclusion size is not greater than 25 µm.

C50 inclusions contain a bulk composition of 35 to 50 vol. percent carbonic liquid (Fig. 12A). Rarely, this fluid inclusions contain accidental opaque daughther minerals. B20 fluid inclusions contain two phases, liquid and vapor, the vapor phase occupies 15 to 20 vol percent of the inclusion and do not contain halite daughther minerals (Fig. 12B). B20H inclusions contain a vapour bubble that occupies 15 to 20 vol. plus halite, in some inclusion of this type is possible to find accidental solid (Roedder, 1984; Fig. 12C), defined based on the different sizes of the solid in the inclusions. B15 fluid inclusions contain liquid plus 10 to 15 vol. percent vapor and lack halite or any opaque daughther minerals at room temperature (Fig. 12D).

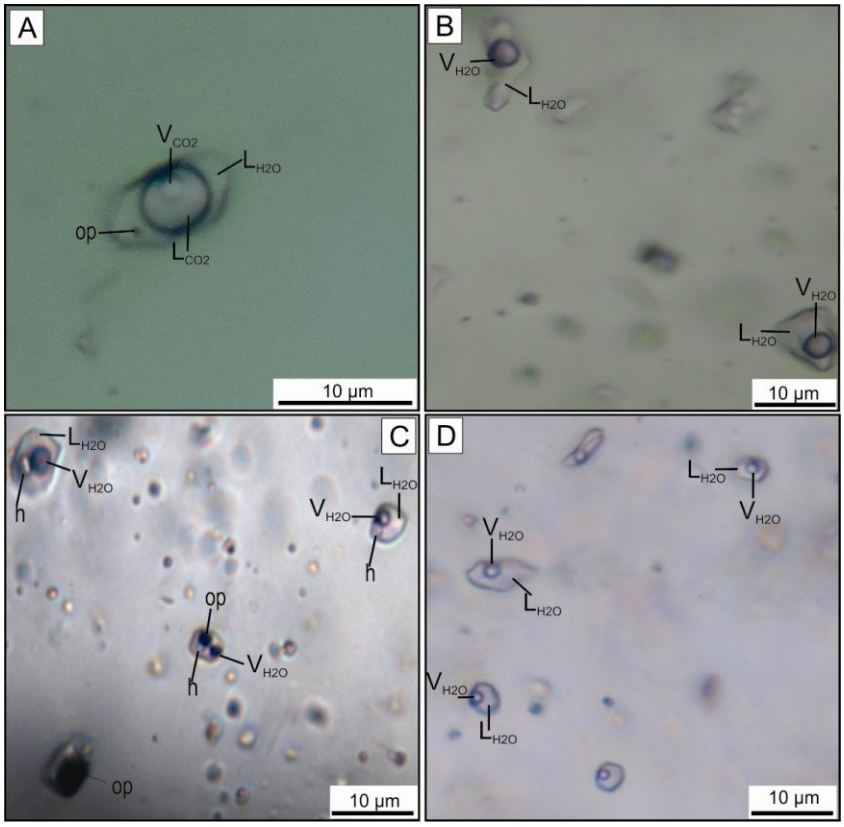

Figure 12. Transmitted light photomicrographs of Juruena fluid inclusions contained in quartz. (A) C50 fluid inclusion with CO_2 containing 50 vol percent bubble and opaque daughter mineral. (B) B20 fluid inclusion containing 20 vol percent bubble. (C) B20H fluid inclusion containing 20 vol percent, halite and accidental opaque mineral. (D) B15 fluid inclusions cotaining 15 or less vol percent. Abbreviations: VCO2 = Vapor CO_2, LCO_2 = Liquid CO_2, LH_2O = Liquid H_2O, VH_2O = Vapor H_2O, op = opaque mineral, h = halite.

The general distribution of the fluid inclusions was defined based on the study of the type the fluid inclusions in the hydrothermal alteration and in the vein types. C50 inclusions dominate in the early stages (stage 1.1), related to K-silicate and a few B20 type fluid inclusions are observed. B20 are dominant in the stage 1.2, where C50 dissapear, a very small proportion of B20H type is founded in this veins. In stage 2.1, related with sericitic alteration, B20 and B15 types fluid inclusions are dominant, in this stage also is possible to recognize halite-bearing fluid inclusions (B20H), a little more in comparisson with stage 1.2. Only B15 type is dominant in the stage 2.2.

Microthermometry Results

The Microthermometry results for the different types of fluid inclusions are summarized in Table 5 and Figs. 13 and 14.

C50 inclusions: The melting temperature (Tm_{CO2}) range from -55.8 to -59.9 ^{o}C, suggesting minor amounts of the other components different of CO_2. Clathrate melts between 3.8 to 9.8 ^{o}C, corresponding salinities of 0.6 to 11.3 wt% NaCl equiv. (Figs. 13 and 14; Table 5). All the fluid inclusions homogenize mainly to liquid and some to vapor between 341 to 456 ^{o}C (Fig. 13), with the carbonic temperature homogenized to liquid at temperatures between 20.1 -30.1 ^{o}C. Their densities range from 0.55 - 0.80 g/cm^3.

Table 5. Microthermometric results of fluid inclusions of the Juruena gold deposit

Inclusion Type	Tm_{CO2} (°C)	T_e (°C)	Tm_{ice} (°C)	Tm_{cla} (°C)	Tm_{halite} (°C)	T_h (°C)	Salinity (WT% NaClequiv)	Density (g/cm^3)
C50 n = 53	-55.8 to -59.9			3.8 - 9.8		341 - 456	0.6 - 11.3	0.55-0.80
B20 n = 58		-21.8 to -36.0	-1.0 to -12.1			280 - 385	1.7 - 16.1	0.86-0.99
B20H n = 16					185 - 264	239 - 349	31.4 – 36.0	0.90-0.92
B15 n = 78		-20.1 to -29.0	-0.5 to -12.9			155 - 285	0.4 - 13.7	0.9-1.02

B20 inclusions: First melting temperature range between –21.8 to -36.0 ^{o}C, indicating presence of dissolved salts beside NaCl (Sterner and Bodnar, 1984). Salinity range from 1.7 to 16.1 wt% NaCl equiv. (Figs. 13 and 14; Table 5). Homogenization temperature ranges from 280 to 385 ^{o}C (Fig. 13; Table 5). The formation of clathrate was observed in a few fluid inclusions, indicating the presence of CO_2, however as the information is limited, we used only the Tm_{ice} to calculate the salinity.

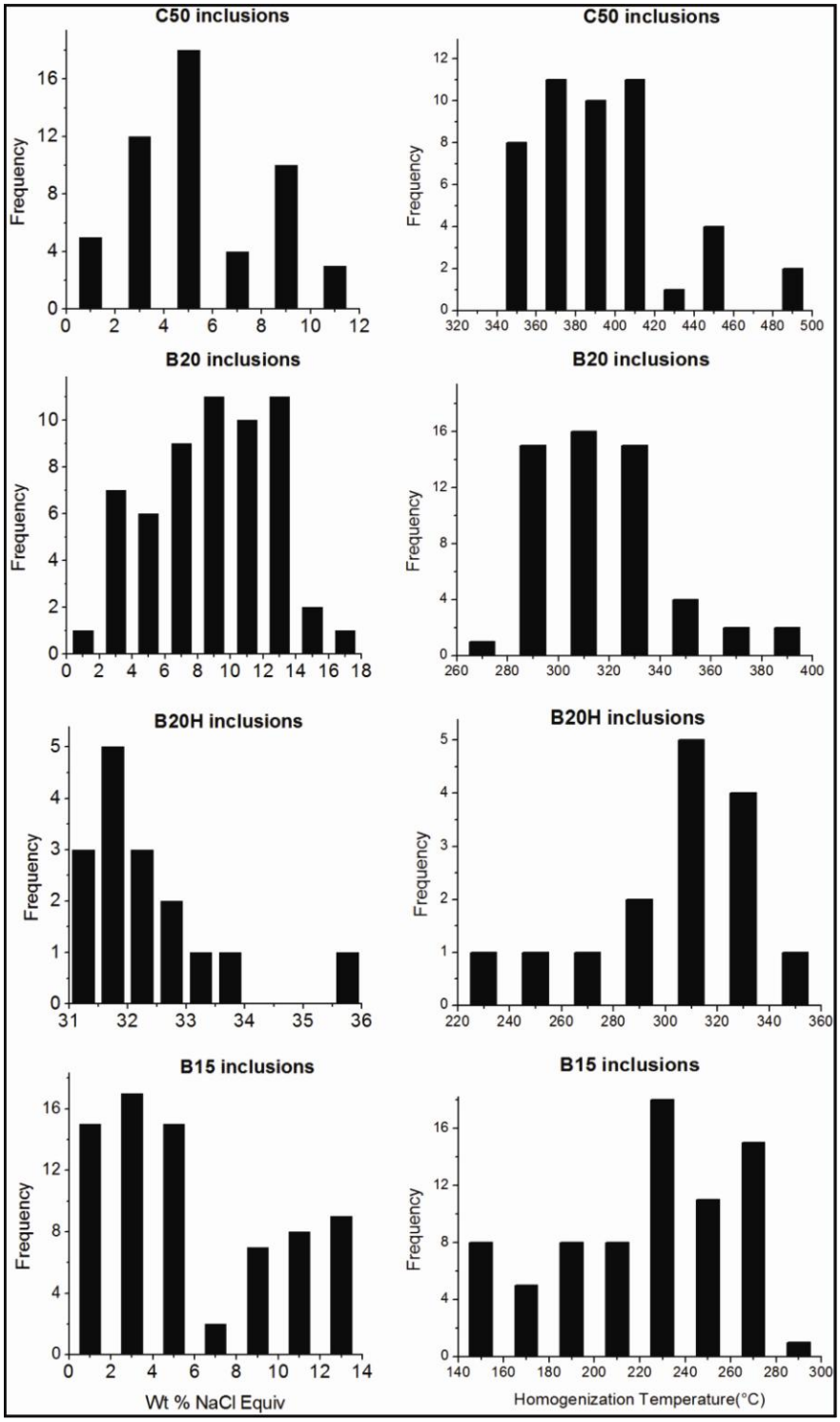

Figure 13. Histograms showing calculate salinities and homogenization temperatures for all inclusion types.

B20H inclusions: Daughter halite dissolves between 185.0 - 264.0 °C (Table 5), corresponding to salinities of 31.4 to 36.0 1 wt% Na Cl equiv. (Fig. 13). All the fluid inclusion homogenized after halite dissolution between 239 – 349 °C.

B15 inclusion: Eutectic temperature measurement range from -21.5 to -29 °C that indicate a salinity range between 0.5 and 12.9 wt% Na Cl equiv. (Fig. 13; Table 5). Homogenization temperature ranges from 155 to 285 °C (Figs. 13 and 14), with a density of 0.9 to 1.02 g/cm^3.

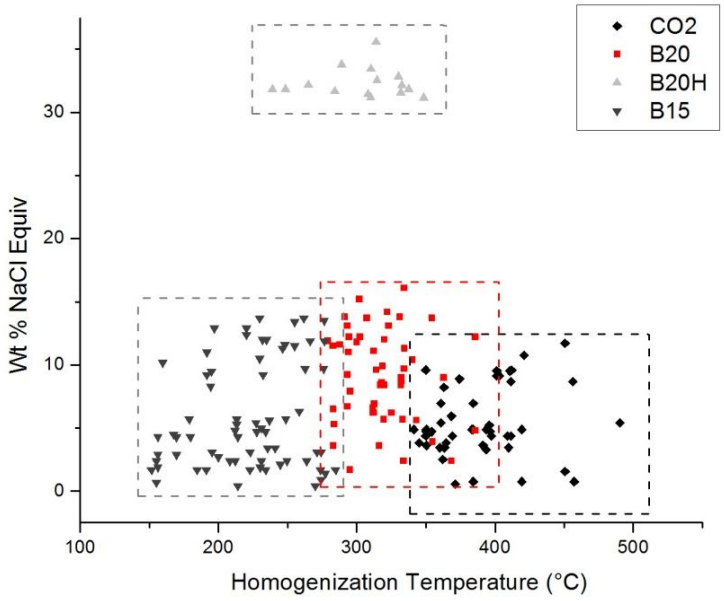

Figure 14. Homogenization temperature versus salinities of the individual inclusions from all the inclusion types in which both measurements were made. Dashed boxes show the entire range of salinities and homogenization temperature for each inclusion type.

Oxygen Isotopes

Eleven quartz samples were analyzed from different stages in the Juruena gold deposit (Table 6): four samples from substage 1.1; three sample from substage 1.2; one sample from substages 2.1 and another one from substage 2.2; and two samples from stage 4. Assuming an equilibrium between the fluid and quartz, the $\delta^{18}O_{fluid}$ values of the hydrothermal fluid were calculated using the equation of Clayton et al., (1972) at the estimated average temperatures for each stage from the microthermometric analysis. The temperatures for substage 1.1, 1.2, 2.1 and 2.2 are respectively, 398, 332, 317, and 220 °C (Table 6). Oxygen from each stage display a similar range in isotopic composition, although it slightly decrease from substage 1.1 (4.88 to 6.87‰) to stage 3 (0.49‰).

TABLE 6. Oxygen Isotope composition of quartz and hydrothermal fluids

Sample ID	Stage	Average homogenization temperature	$\delta^{18}O_{V\text{-}SMOV}$ (‰)	$\delta^{18}O_{fluid}$ (‰)
40	1.1	398	9	4.88 ± 0.9
57	1.1		11.3	6.87 ± 0.9
66	1.1		9.3	5.18 ± 0.9
61	1.1		10.5	6.37 ± 0.9
43	1.2	332	9.9	4.08 ± 0.2
53	1.2		10.4	4.57 ± 0.2
79	1.2		10.4	4.57 ± 0.2
70	2.1	317	10.7	4.38
78	2.2	220	10.5	0.49
56	4		12.7	
81	4		12.4	

Electron Probe Microanalysis (EPMA)

A total of 135 spots were made in order to quantify trace elements content of the different pyrites generation and their relationship with gold mineralization. Gold is detectable in almost all analyzed pyrite samples, showing very high values for py2 and py3 (0.03 wt%; Table 7), indicating that gold likely occurs primarily as micro-sized inclusions in the pyrite (see below; Fig. 10A). Gold concentration in the other generations (py1 and py4), is mostly below detection limit. Py1 has the highest As concentration (0.04 wt%) in comparison with the other generations, where this elements is mainly below detection limit. Most of the samples are depleted in Te and Sb, while some individual crystal present low concentration. This condition difficults to establish a clear relationships with gold

Thallium is the most abundant element in all the pyrites. The element characteristic and the constant pattern in all the pyrite types suggest that thallium is included in pyrite lattice.

Table 7. Selected EPMA analyses (wt%) in pyrite. Bdl = below detection limit. Detection limits (wt%) are shown below each element.

Type of pyrite	SAMPLE	LINE	Sulfide type	Cu (0.04)	Fe (0.01)	As (0.02)	S (0.01)	Sb (0.02)	Te (0.02)	Au (0.02)	Tl (0.03)	TOTAL
Py1 n = 31	Un 9 40-t10	76	Py_1	0.06	46.16	bdl	53.56	bdl	bdl	bdl	0.06	99.84
	Un 4 40-t6	65	Py_1	0.04	45.96	bdl	53.71	bdl	bdl	bdl	bdl	99.74
	Un 41 66-t34	153	Py_1	0.04	46.36	bdl	53.88	bdl	bdl	bdl	bdl	100.29
	Un 36 58-t49	134	Py_1	bdl	44.86	0.04	54.17	bdl	bdl	bdl	bdl	99.10
	Un 36 58-t49	135	Py_1	0.41	44.59	0.02	53.66	bdl	bdl	bdl	0.03	98.73
	Un 36 58-t49	137	Py_1	0.06	44.74	bdl	53.70	bdl	bdl	bdl	bdl	98.53
	Un 37 58-t50	141	Py_1	0.71	46.21	bdl	53.38	bdl	bdl	bdl	bdl	100.32
	Un 9 40-t10	76	Py_1	0.06	46.16	bdl	53.56	bdl	bdl	bdl	0.06	99.84
	Un 4 40-t6	65	Py_1	0.04	45.96	bdl	53.71	bdl	bdl	bdl	bdl	99.74
	Un 41 66-t34	153	Py_1	0.04	46.36	bdl	53.88	bdl	bdl	bdl	bdl	100.29
Py2 n = 33	Un 50 50-t13	174	Py_2	bdl	46.70	bdl	51.87	bdl	bdl	bdl	0.04	98.63
	Un 50 50-t13	177	Py_2	bdl	46.85	bdl	51.89	bdl	bdl	0.02	bdl	98.78
	Un 51 50-t16	181	Py_2	bdl	46.75	bdl	51.67	bdl	bdl	0.02	0.03	98.50
	Un 52 50-t15	187	Py_2	bdl	46.30	bdl	52.90	bdl	bdl	0.02	bdl	99.25
	Un 52 50-t15	188	Py_2	bdl	46.78	bdl	52.57	bdl	bdl	0.02	bdl	99.38
	Un 52 50-t15	190	Py_2	bdl	46.39	bdl	51.96	bdl	bdl	0.03	bdl	98.41
	Un 54 50-p2	197	Py_2	0.07	46.38	bdl	53.60	bdl	bdl	0.02	0.03	100.10
	Un 54 50-p2	198	Py_2	bdl	46.46	bdl	51.97	bdl	bdl	0.02	0.03	98.48
	Un 58 50-t22	212	Py2	bdl	45.93	bdl	53.46	bdl	bdl	bdl	0.04	99.45
Py3 n = 40	Un 60 75-t59	223	Py_3	bdl	46.57	bdl	53.08	bdl	bdl	0.02	0.03	99.70
	Un 61 75-t46	232	Py_3	bdl	46.56	bdl	53.70	bdl	bdl	0.02	0.03	100.31
	Un 60 75-t59	229	Py_3	bdl	46.88	0.02	53.45	bdl	bdl	0.03	0.04	100.42
	Un 61 75-t46	232	Py_3	bdl	46.56	bdl	53.70	bdl	bdl	0.02	0.03	100.31
	Un 61 75-t46	233	Py_3	bdl	46.87	bdl	53.86	bdl	bdl	0.02	0.05	100.81
	Un 62 75-t45	234	Py_3	bdl	46.68	bdl	53.84	bdl	bdl	0.02	bdl	100.55
	Un 63 75-t56	238	Py_3	bdl	46.80	bdl	53.88	bdl	bdl	0.02	0.04	100.75
	Un 63 75-t56	241	Py_3	bdl	46.76	bdl	54.07	bdl	bdl	0.03	bdl	100.88
	Un 63 75-t56	242	Py_3	bdl	46.71	bdl	53.69	bdl	bdl	0.03	0.04	100.47
Py4	Un 23 26-p1	102	Py_4	bdl	46.86	bdl	53.74	bdl	bdl	bdl	0.05	100.67

n = 24	Un 24 26-Black	105	Py_4	0.05	46.39	bdl	53.99	bdl	bdl	bdl	0.03	100.48
	Un 27 26-t24	112	Py_{4rim}	0.05	46.58	bdl	54.11	bdl	bdl	bdl	0.03	100.79
	Un 28 26-t24	114	Py_{4core}	bdl	46.57	bdl	53.86	bdl	bdl	0.02	0.03	100.49
	Un 31 26-t31	119	Py_4	0.04	46.74	bdl	53.89	bdl	bdl	bdl	0.05	100.73
	Un 32 26-t2	121	Py_4	bdl	46.70	bdl	54.00	0.02	bdl	0.02	bdl	100.78
	Un 32 26-t2	122	Py_4	bdl	46.47	bdl	54.18	bdl	bdl	0.03	0.04	100.72
	Un 59 75-t58	220	Py_4	bdl	46.43	bdl	52.95	bdl	bdl	bdl	0.05	99.43
	Un 59 75-t58	222	Py_4	bdl	46.44	bdl	52.85	bdl	bdl	bdl	bdl	99.30
	Un 63 75-t56	237	Py_4	bdl	46.60	bdl	53.89	bdl	bdl	bdl	bdl	100.50

Copper concentration is lower than detection limit in almost all the pyrites, except in the first generation, where the concentrations are very high.

Electron microprobe analyses of py1 indicate a poor concentration of trace elements (As <0.04, Sb, Au and Te below detection limit; Table 7). Copper is the principal element in this generation (Cu = 0.71wt%; Fig. 15A).

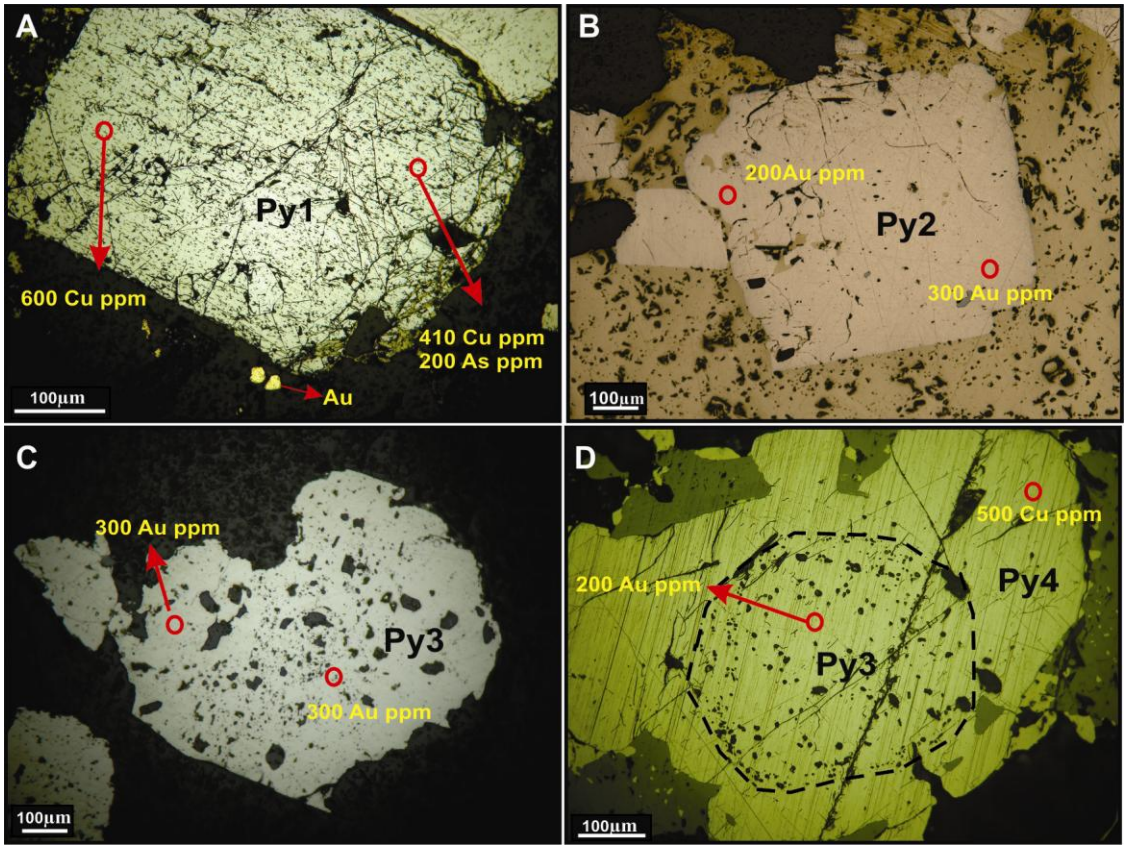

Figure 15. EPMA Spots analysis of selected pyrites. Plane-polarized reflected light. See how gold concentration progressively increases, from euhedral gold-depleted Cu-rich py1 (A), through sub-rounded py2 (B) with both elements in different concentrationsup to anahedral porous gold-rich Cu-depleted py3 (C). Copper has inverse behavior; Cu-richest pyrite is the first generation (A). (D) Depleted in gold py4 with core of Au-rich py3.

Py2 is depleted in all trace metals, showing a decrease in As and a more important gold concentration (Au <0.03wt %; Fig. 15B). The Au/Cu ratio is opposite to py1. In this group of pyrite, gold concentration is high and Cu concentration is low. EPMA results in py3 present similar behavior with py2. Gold concentration in this pyrite generation is higher than in the others (Au= 0.035 wt%; Fig. 15C). The last generation, py4 is depleted in almost all the analyzed elements. Observed variations in the internal texture of py4 aggregates include a core broken and corroded crystals of py3 with a rim of py_4 (Fig. 10D and 15D). This texture suggests that the hydrothermal pyrite was recrystallized from preexisting hydrothermal pyrite. The porous have been filled by silicates. The cores of these crystals are enriched in gold and depleted in copper, and the rims are depleted in both, exceptionally the rims can contain Cu concentration (Fig. 15D).

Discussion

Timing of Magmatism and Mineralization

The results of the U-Pb (1790 ± 6 Ma and 1792 ± 5.8 Ma) and Re-Os (1805 ± 7.0 Ma) of the early monzogranite, late micromonzogranite, and the molybdenite, respectively, do not show a clear overlapping between the magmatism and mineralization ages (taking into account the uncertainties). However, is possible to suggest a relationships between the felsic magmatism of the Paranaíta Intrusive Suite, developed between 1819 to 1793 (Santos et al., 2008), and gold mineralization in the Juruena deposit.

The results reported in this work could be explained with a model in which the mineralization at Juruena gold deposit is the result of a single large intrusive event that produced rock with the same composition but different textures together with the hydrothermal alteration. This process is clearly related to the evolution of the Paranaíta Intrusive Suite that is interpreted as the causative rock of the gold mineralization.

The new geochronological data has a very important metallogenic implication, because other deposits with similar mineralization ages have been previously reported in the eastern part of the Alta Floresta Gold Province (1782 to 1792 Ma; Xavier et al., 2013). These results open the possibility to relate the gold mineralization in the province with a single metallogenic event, associated with felsic magmatism of the Paranaíta Intrusive Suite, creating new perspectives for gold exploration in the province.

Sources and Fluid Evolution

The $\delta^{34}S_{sulfide}$ values from the different stages in Juruena gold deposit range between -7.8 and +1.5‰ (Table 4). The evolution of this hydrothermal system is characterized by the gradually increase of $\delta^{34}S_{sulfide}$ values, where the lowest are related with earliest events (Stage 1.1 and 1.2), and the highest values with the late stage (Stage 3), defining a spatial zonation pattern (Fig.16). According to Ohmoto and Rye, (1979), low $\delta^{34}S_{sulfide}$ values could be explained by two different ways: (1) magmatic- hydrothermal processes or (2) incorporation of an external, isotopically light sulfur source (sedimentary sulfide). Base on our observations, the wallrocks in Juruena deposit are devoid of sedimentary sulfides, so the possibility of an incorporation of any sedimentary sulfide is difficult. On other hand, the close relationship between gold mineralization and granitic rocks, together with the small possibility of sedimentary sulfide presence, are a clear

evidence to concluded that sulfide at Juruena deposit is mainly of oxidized magmatic source (Ohmoto and Rye, 1979), that could be associated with oxidized I-type granites from the Paranaita Intrusive Suite.

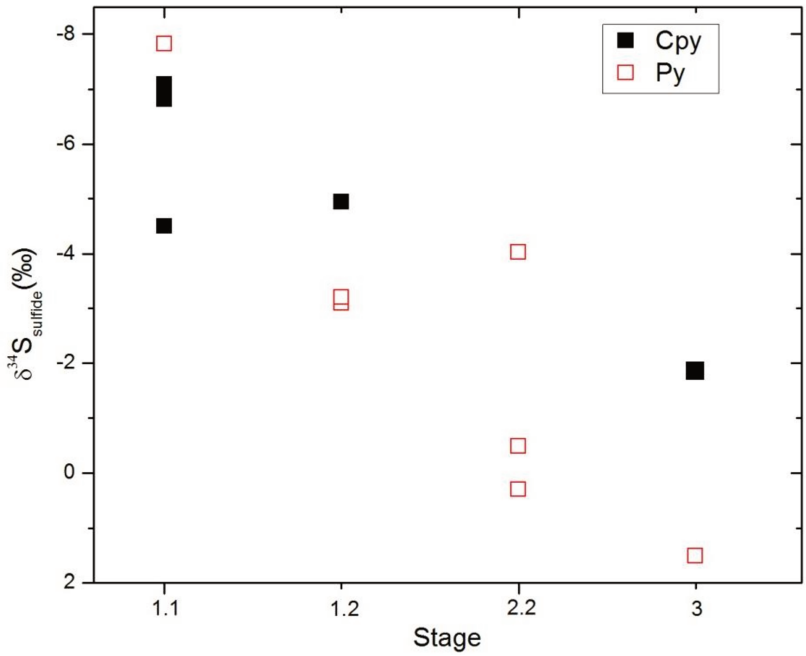

Figure 16. Evolution of the $\delta^{34}S_{sulfide}$ composition from the different stages in the Juruena gold deposit. Abbreviation: cpy = chalcopyrite, py = pyrite.

The spatial zonation pattern observed in Juruena deposit, cannot be simply explained by sulfide deposition via cooling oxidized magmatic-hydrothermal fluid (cooling would produce an opposite trend; Rye 1993). Progressively enrichment of $\delta^{34}S_{sulfide}$ composition from the earliest to latest stages suggests that redox processes were important during sulfide deposition and, our observed pattern could be caused by progressive reduction of sulfate-rich, metal-bearing fluids with distance upwards and outwards from the earliest stages (Deyell 2005; Wilson et al., 2007). Similar isotopic zonation has been reported principally at some porphyry deposits (e.g., Mt Polley alcalic porphyry: Delley, 2005; Cadia district: Wilson et al., 2007).

Fluid Evolution

The isotopic and fluid inclusion data provide insights to determine the nature and evolution of the fluid system in the Juruena gold deposit. The occurrences of different types of fluid inclusions, and their distribution in the stages studied (stage 1 and 2), suggest that the deposit was formed by an initial CO_2-H_2O-NaCl system, in which CO_2 gradually scape until it produced an H_2O-NaCl system, probably result of the immiscibility of the fluids.

Temperature at Juruena deposit gradually decreases from early to late mineralized stages, but the salinities did not display marked variations (Table 5; Fig. 13-14), except for the high salinities from B20H type in stage 2.1. This characteristic suggests that hydrothermal fluids were exsolved probably from magmatic sources, weakly mixed with meteoric fluids (substage 2.2).

Calculated $\delta^{18}O_{fluid}$ values for the different stages in the deposit were plotted in Fig. 17, where is possible to note that $\delta^{18}O_{fluid}$ values regularity decrease from stage 1.1 ($\delta^{18}O_{fluid}$ = 4.88 to 6.38‰) to stage 2.2 ($\delta^{18}O_{fluid}$ = 0.49‰). Fluids in stages 1.1, 1.2 and 2.1 suggest a predominant magmatic derivation (e.g., Taylor, 1979; Sheepard, 1986; Giggenbach, 1992), while the low $\delta^{18}O_{fluid}$ value in stage 2.2 could be the result of the mixture of initial magmatic fluids with meteoric waters (Taylor, 1979).

Origin of the CO_2-rich fluid inclusions in magmatic-hydrothermal systems could be explained in the following way: magmatic-derived carbon dioxide is likely more abundant in deeper crustal environments, because it is less soluble than water and other volatiles (Fogel and Rutherford, 1990). The low solubility of carbon dioxide results in the early exsolution of CO_2 and H_2O at much higher pressure in comparison with chlorine (Giggenbanch, 1997; Lowestern, 2000 and 2001). During the upward intruding process of magma, chlorine would be immiscible and exsolved from CO_2-bearing magma after CO_2 and H_2O. It is therefore concluded that CO_2-bearing magma firstly generated low salinity CO_2-rich fluids and subsequently, moderate to high salinity fluids (Shinohara and Kazahyo, 1995).

The proposed CO_2-H_2O-NaCl, and H_2O-NaCl from a magmatic source for the fluids related with gold mineralization have been also reported in many mineral porphyry deposits (e.g., Butte porphyry Cu-Mo deposit: Rusk and Reed, 2008; Bingham Canyon porphyry Cu-Mo-Au deposit: Landtwing et al., 2010; Nannihu giant porphyry Mo-W deposit: Yang et al., 2012) and intrusion related gold deposit (Baker, 2002).

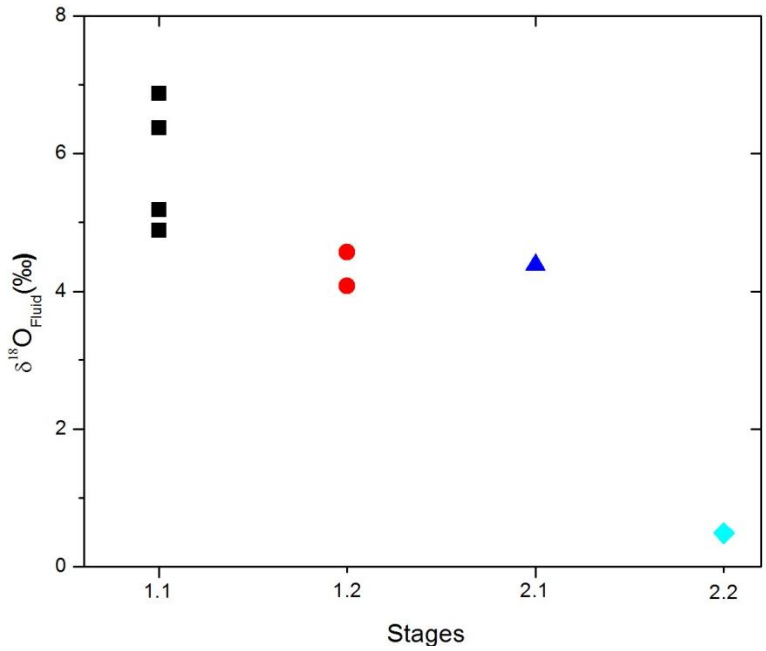

Figure 17. Evolution of the $\delta^{18}O_{fluid}$ composition from the different stages in Juruena gold deposit.

Chemical composition of Pyrite

According to the EPMA results, the different type of pyrites show some similarities and differences in elemental composition, that provide evidence to recognize the characteristics of the several events and their importance in gold distribution.

At the Juruena gold deposit Cu, Au, and Tl are the most abundant elements in all the pyrite generations. The results reveal a non clear correlation between the analyzed elements (Table. 7). Copper and gold elements present an opposite behavior in the deposit, richest copper pyrites (py1) are depleted in gold, while Au-richest crystals are depleted in copper (py3; Fig. 15A-C). In the py2 both elements could be observed in variables concentrations (Fig. 15B). A high gold value is related to anhedral, very porous pyrites (py3; 15C), while Cu is predominantly in the euhedral py1 crystals.

Gold richest porous pyrite could be a consequence of different dissolution-precipitation reactions during the evolution of the hydrothermal system (Putnis, 2002). This process would dissolve and redistribute any trace element in the pyrites and eventually precipitate as nano-micro-size particles (Fig. 10A-D). In the case of gold, that is highly susceptible to small-scale mobilization under a range of conditions, dissolution-precipitation reaction creates a unique distribution pattern within each grain of pyrite (Cook et al., 2012).

The high content of copper reported in pyrites from Juruena gold deposit, which can reach up to 0.71 wt%, could occur in two dominant mineralogical forms: (1) Cu structural bound, and (2) micro- to nano sized particle inclusions of chalcopyrite. The $Cu^{2+} \leftrightarrow Fe^{2+}$ within the pyrite structure is highly unlike, because any relationships between these elements was defined (Table. 7; Shimazaki and Clark, 1970; Schmid-Beurmann and Bente, 1995), for this reason we reject the first possibility, concluding that copper appearing as micro-inclusions within the pyrite, is a more suitable possibility.

Gold concentrations are variable in the analyzed pyrites (ppb up to 345 ppm). A correlation between gold and arsenic dissolved in pyrite has been reported in different gold deposits types, including Carlyn-type, epithermal and orogenic gold deposits (e.g., Cook and Chryssouilis, 1990; Reich et al., 2005; Deditus et al., 2009; Large et al., 2006; Large et al., 2009). According to the results was not possible to defined the relationship between gold and arsenic in the mineral deposit, because the As concentration is below detection limit in almost all the samples. For these reason we assume that the presence of invisible gold in Juruena is irrelevant because the pyrite do not contain any significant As. The result here is inconsistent with previous hypothesis, where the recognition of arsenic alone is very important into the incorporation of gold and silver in the pyrite (Cook and Cryssouilis, 1990; Simmon et al., 1999; Reich et al., 2005; Deditus et al., 2011; Reich et al., 2013). However, the As-dependent in cases where gold and silver appear as particles are also documented (Palenik et al., 2004; Reich et al., 2005; Cook et al., 2009; Deditus et al., 2011). The highest gold concentration obtained in microprobe analysis could be explained if the gold is present as micro- to nano-size particles (Au^0; Reich et al., 2005). Individual particles of free gold were observed in crystals of pyrites (Fig. 5A-C) and in SEM analysis, where a Au-telluride association was recognized (Fig. 5D), coinciding with the presence of gold as Au^0.

According to this results is possible define that gold from Juruena is a product of the fluid mixing and repeated pulses in a magmatic hydrothermal environment (Audétat et al., 1999; Heinrich et al., 2004; Reich et al., 2013), that generated large remobilization of gold and posterior precipitation as nano- micro-particles.

Ore Genesis

The Juruena gold deposit can be classified as a porphyry gold deposit. The main supporting elements are presented here: (1) granite-hosted gold mineralization (Juruena Intrusive Suite); (2) the Re-Os age (1805 ± 7 Ma) is consistent with zircon U-Pb ages (1792 ± 6.4 and 1792 ± 5.8 Ma) of the granitic rocks, indicating a close temporal and likely genetic relationship between gold mineralization and magmatism of Paranaita Intrusive Suite; (3) alteration zoning, from K-silicate, through sericitic alteration (phyllic alteration), to propylitic alteration, as shown in Nannihu Mo-W deposit (Yang et al., 2012), Deixing Cu-Mo-Au deposit (Hou et al., 2013), and Yuchiling Mo deposit (Zhang et al., 2013), all of them located in China; (4) the occurrence of veins that shows the same characteristics of veins present in typical porphyry systems (e.g., Gustafson and Hunt, 1975; Sillitoe, 2000; Seedorf et al., 2005); (5) the evidence of CO_2-H_2O-NaCl and NaCl-H_2O fluids. CO_2 fluid inclusions are not common in the porphyry type deposits, although recent studies have indicated that they could appear in porphyry deposits (e.g., Rusk et al., 2008; Landtwing et al., 2010), but this is more common in porphyries formed in continental collision or post-collisional settings (Richards et al., 2005; Tang et al., 2013; Yang et al., 2012); (6) sulfur isotope studies show that ore-forming fluids originally have an oxidized magmatic source with a strong redox control, that generate a zonation during the evolution of Juruena gold deposit (Fig. 16), this behavior has been reported at Mt. Polley Alkali porphyry (Delley, 2005) and Cadia District (Wilson et al., 2007); (7) oxygen isotope results also show a magmatic to magmatic meteoric mixing source for the mineralizing fluid (Fig. 17), characteristic of porphyry systems (e.g., Bajo la Alumbrera Cu-Mo deposit: Ulrich et al., 2002; Serrinha gold deposit: Moura et al., 2006); (8) elemental chemistry in the pyrites do not show a clear relationships between the different analyzed elements, but it was possible to define that gold in the deposit appears as nano– micro-particles precipitated directly from the magmatic-hydrothermal solution (Deditus et al., 2011; Reich et al., 2013).

However some of the characteristics mentioned above have been recognized in typical porphyry deposits, the most important similarities were identified in Chinese deposits, where mineralization is related to Mesozoic granitic rocks (175 to 120 Ma; Mao et al., 2014), hosted in the North China Craton (~3800 Ma). In this Craton the gold metallogeny occurred within the tectonic framework of lithosphere thinning and reactivation of the North China Craton that generated heat and fluid input at the same time that promoted favorable structures for fluid flow

and gold deposition (Li et al.,2013). These mineral deposits also have been classified, mainly, as porphyry deposits.

By the proximal relationship with granitic rocks, Juruena gold deposit could be also classified as Intrusion Related Gold Deposit (IRGD). Important differences between Juruena gold deposit and the typical genetic model purposed to describe the IRGD have been recognized, referring to: geological setting, ore paragenesis, geochemistry feature, alteration mineralogy and zonation, (Thompson et al., 1999; Goldfarb et al., 2005; Hart, 2007).

Conclusions

The Juruena gold deposit is hosted by oxidized I-type granites of Paranaita Intrusive Suite (U-Pb age 1790 ± 6.4 Ma and 1792 ± 5.8 Ma). The deposit formed at 1805 ± 7 Ma (Re-Os age model of one molybdenite sample coexisting with Au-bearing pyrite). Isotopic data (oxygen and sulfur) from different stages suggest a magmatic sources for the early mineralized CO_2-H_2O-NaCl fluids with addition of meteoric waters in the late stage. During the upward intruding process, magma lost CO_2 and formed the NaCl-bearing and NaCl-H_2O fluid inclusions that formed the sericitic hydrothermal alteration. In the last stage the mixture of fluids promoted the formation of H_2O-NaCl fluids with low temperatures.

Gold is primarily located within quart-sulfide veins and calcite sulfide veins. In the first case gold appears related to veins that represent substage 1.1, present in the K-silicate hydrothermal alteration. In calcite-sulfide veins gold is related with stage 3. Occasionally gold occurs with disseminated sulfides in the altered sericitic host rocks. In general, gold appear as nano- size-particles in the different types of pyrites, as free gold or filling fractures and associated with tellurides. Trace element geochemistry did not show any relationship between the different studied elements, we interpreted this as a result of the intensive and repeated pulses of magmatic-hydrothermal origin.

Based on the results, the Juruena gold deposit is most similar to relatively Au-porphyry system formed by a single magmatic hydrothermal event. This research converts the Paranaíta Intrusive Suite in a very important target for gold mineral exploration in the Alta Floresta Gold Province.

REFERENCES

Assis R.R., 2011, Depósitos auríferos associados ao magmatismo granítico do setor lest da Provincia de Alta Floresta (MT),Craton Amazônico: tipologia das mineralizações, modelos genéticos e implicações prospetivas: Unpublished M.Sc. Thesis, Campinas, Brazil. University of Campinas, 456 p.

Audétat, A., Gunther, D., and Heinrich, C. A., 1998, Formation of a magmatic–hydrothermal ore deposit: insights with LA-ICP-MS analysis of fluid inclusions: Science v.279, p. 2091–2094.

Azmy, K., Kendall B., Creaser, R. A., Heaman, L., and de Oliveira, T. F., 2008, Global correlation of the Vazante Group, São Francisco Basin, Brazil: Re–Os and U–Pb radiometric age constraints: Precambrian Research, v.164, p.160–172.

Baker, T., 2002, Emplacement depth and carbon dioxide-rich fluid inclusions in intrusion-related gold deposit: Economic Geology, v. 97, p. 1111–1117.

Black, L.P., Kamo, S.L., Allen, C.M., Aleinikoff, J.N., Davis, D.W., Korsch, R.J., Foudoulis, C., 2003, TEMORA 1: a new zircon standard for Phanerozoic U–Pb geochronology: Chemical Geology, v. 200, p.155-170.

Bodnar, R.J., 1993, Revised equation and table for determining the freezing point depression of H2O-NaCl solutions: Geochimica et Cosmochimica Acta, v. 57, p. 683–684.

Clayton, R. M. The use of bromide pentafluoride in the extraction of oxygen from oxides and silicates for isotopic analysis: Geochemiestry and Cosmochemistry Acta, v. 27. p. 47-52.

Clayton, R.N., O'Neil, J.R., and Mayeda, T.K., 1972, Oxygen isotope exchange between quartz and water: Journal of Geophysical Research, v. 77, p. 3057–3067.

Collins, P.L.F., 1979, Gas hydrates in CO2-bearing fluid inclusions and the use of freezing data for estimation of salinity: ECONOMIC GEOLOGY, v. 74, p.1435–1444.

Cook, N.J., Chryssoulis, S.L., 1990, Concentration of "invisible gold" in the common sulfides: The Canadian. Mineraogist. v. 28, p.1–16.

Coplen, T.B., Hopple, J.A., Böhlke, J.K., Peiser, H.S., Rieder, S.E., Krouse, H.R., Rosman, K.J.R., Ding, T., Vocke, Jr., R.D., Revesz, K.M., Lamberty, A., Taylor, P., and De Bièvre, P., 2002, Compilation of minimum and maximum isotope ratios of selected elements in naturally occurring terrestrial materials and reagents: U.S. Geological Survey Water-Resources Investigations. Report 01-4222, 98p.

Creaser, R. A., Papanastassiou, D. A. and Wasserburg, G. J., 1991, Negative thermal ion mass spectrometry of osmium, rhenium, and iridium: Geochimica and Cosmochimica Acta, v. 55, p. 397–401.

Deditius, A., Utsunomiya, S., Ewing, R.C., Chryssoulis, S.L., Venter. D., and Kesler, S.E., 2009, Decoupled geochemical behaviour of As and Cu in hydrothermal systems: Geology, v.37, p. 707-710.

Deditus, A.P., Utsunomiya, S., Reich, M., Kesler, S.T., Ewin, R.C., Hough, R., and Walshe, J., 2011, Trace metal nanoparticles in pyrite: Ore Geology Reviews, v.42, p. 32-46.

Deng, P., Ren, J.S., Ling, H.F., Shen, W.Z., Sun, L.Q., Zhu, B., and Tan, Z.Z., 2012, SHRIMP zircon U-Pb ages and tectonic implication for Indonesian granitoids of southern Zhuguangshan granitic composite, South China: Chinese Science Bulletin, v. 57, p. 1542-1552.

Deyell, C.L., 2005, Sulfur isotope zonation at the Mt Polley alkalic porphyry Cu-Au deposit, British Columbia, Canada: Mineral Deposit Research: Meeting the Global Challenge, China, 18-21 August, Proceedings, p. 373-376.

Duarte, B.T., Rodrigues, B.J., Riveiro, E.P.S., and Scandolara, J.E., 2012, Tectonic evolution of the Juruena magmatic arc between the Aripuanã and Juruena Rivers: nortwest Mato Grosso State, Brazil: Revista Brasileira de Geociências, v. 42(4), p. 824-840.

Fogel, R.A., and Rutherford, M.J., 1990, The solubility of carbon dioxide in rhyolitic melts: A quantitative FTIR study: American Mineralogist, v. 75, p. 1311–1326.

Giesemann, A., Jager, H.J., Norman, A.L., Krouse, H.R., and Brand W.A., 1994, On line sulfure isotope determination using an elemental analyser coupled to a mass spectometer: Analytical Chemistry, v.66, p. 2816-2819.

Giggenbach, W.F., 1992, Isotopic shifts in waters from geothermal and volcanic systems along convergent plate boundaries and their origin: Earth and Planetary Science Letters, v. 113, p. 495–510.

Giggenbach, W.F., 1997, The origin and evolution of fluids in magmatic-hydrothermal systems, in Barnes, H.L., ed., Geochemistry of hydrothermal ore deposits, 3rd edition: New York, John Wiley and Sons, Inc., p. 737–796.

Goldfarb, R.J., Baker, T., Dubé, B., Groves, D.I., Hart, R.C.J., and Gosselin, P., 2005, Distribution, character, and genesis of gold deposits in metamorphic terranes: ECONOMIC GEOLOGY 100TH ANNIVERSARY VOLUME. p.407-450.

Goldstein, R.H., and Reynolds, T.J., 1994, Systematics of fluid inclusions in diagenetic materials: Society for Sedimentary Geology Short Course 31, 199 p.

Gustafson, L.B., and Hunt, J.P., 1975, The porphyry copper deposit at El Salvador, Chile: ECONOMIC GEOLOGY, v. 70, p. 857–912.

Hart, J.R.C., 2007, Reduced intrusion-related gold system, in Goodfellow, W.D., Mineral deposit of Canada: Synthesis of major deposit types, distric metallogeny, the evolution of geological provinces and exploration methods: Geological Association of Canada, . Mineral deposit division, Special publication No. 5, p. 95-112.

Heinrich, C. A., Driesner, T., Stefánsson, A., and Seward, T. M., 2004, Magmatic vapour contraction and the transport of gold from porphyry environment to epithermal ore deposits: Geology, v.32, p. 761–764.

Hou,Z., Pan,X., Li, Q., Yang, Z., and Song, Y., 2013, The giant Dexing porphyry Cu–Mo–Au deposit in east China: product of melting of juvenile lower crust in an intracontinental setting: Mineralium Deposita, v.48, p.1019-1045.

Junior, A.S., 2012, Tipo e distribução da alteração hidrotermal no depósito aurífero de Pé Quente, setor lesta da Provincia Aurífera de Alta FLoresta (MT): Universidade Estadual de Campinas; Trabalho de Conclusão de Curso; 81p.

Landtwing, M.R., Furrer, C., Redmond, P.B., Pettke, T., Guillong, M., Heinrich, C.A., 2010. The Bingham Canyon porphyry Cu–Mo–Au deposit. III. Zoned copper–gold ore deposition by magmatic vapor expansion: ECONOMIC GEOLOGY, v.105, p.91–118.

Large, R. R., Danyushevsky, L. V., Hollit, C., Maslennikov, V., Meffre, S., Gilbert, S. E., Bull, S., Scott, R. J., Emsbo, P., Thomas, H., Singh, B. and Foster, J., 2009, Gold and trace element zonation in pyrite using a laser imaging technique: implications for the timing of gold in orogenic and Carlin-style sedimenthosted deposits: ECONOMIC GEOLOGY, v.104, p. 635–668.

Large, R.R., Maslennikov, V.V., Robert, F., 2006, Multistage sedimentary and metamorphic origin of pyrite and gold in the giant Sukhoi Log deposit, Lena Gold Province, Rusia: ECONOMIC GEOLOGY, v. 102, p. 1233-1267.

Lawley, C. J. M., Richards, J. P., Anderson, R. G., Creaser, A., and Heaman, L. M., 2010, Geochronology and Geochemistry of the MAX Porphyry Mo Deposit and its Relationship to Pb-Zn-Ag Mineralization, Kootenay Arc, Southeastern British Columbia, Canada: ECONOMIC GEOLOGY, v.105, p. 113-1142.

Li, X.C., Fan, H.R., Santosh, M., Hu, F.F., Yang, K.F., and Lang, T.G., 2013, Hydrothermal alteration associated with Mesozoic granite-hosted gold mineralization at the Sanshandao deposit, Jiadong Gold Province, China: Ore Geology Reviews, v. 53, p. 403-421.

Lowenstern, J.B., 2000, A review of the contrasting behavior of two magmatic volatiles: Chlorine and carbon dioxide: Journal of Geochemical Exploration, v. 69–70, p. 287–290.

——2001, Carbon dioxide in magmas and implications for hydrothermal systems: Mineralium Deposita, v. 36, p. 490–502.

Ludwig, K. 2003, User's Manual for Isoplot 3.00: A Geochronological Toolkit for Microsoft Excel. Berkeley Geochronology Center Special Publication 4.

Mao, J., Pirajno, F., Lehmann, B., Luo, M., and Berzina, A., 2014, Distribution of porphyry deposits in the Eurasian continent and their corresponding tectonic settings: Journal of Asian Earth Sciences, v. 79, p. 576-584.

Miguel, Jr.E. 2011, Mineralizações auríferas do lineamento Peru-Trairão, Provincia aurífera de Alta Floresta - MT: controle estrutural e idade U-Pb das rochas hospedeiras. Qualificação - Dissertação de Mestrado, Instituto de Geociências Universidade Estadual de Campinas, 86 p.

Moura, M.A., Botelho, N.F., Olívio, G.R., Kyser, T.K., 2006, Granite-related Paleoproterozoic, Serrinha gold deposit, Southern Amazonia, Brazil: hydrothermal alteration, fluid inclusion and stable isotope constraints on genesis and evolution: ECONOMIC GEOLOGY, v. 101, p.585-605.

Ohmoto, H., and Rye, R.O., 1979, Isotopes of sulfur and carbon, in Barnes, H.L., ed., Geochemistry of hydrothermal ore deposits, 2nd ed.: New York, Jhon Wiley & Sons, p.509-567.

Oliveira, C.C., and Albuquerque, M. C., 2003, Programa Levantamentos Geológicos Básicos do Brasil - PLGB. Projeto Província Mineral de Alta Floresta (PROMIN Alta Floresta). Geologia e Recursos Minerais da Folha Alta Floresta-SC.21-Z-X-C. Brasília: CPRM, 2003.

Paes de Barros, A. J., 2007, Granitos da região de Peixoto de Azevedo - Novo Mundo e mineralizações auríferas relacionadas - Provincia Aurífera Alta Floresta (MT): Unpublished Phd. Thesis, Campinas, Brazil. University of Campinas, 171 p.

Palenik, C.S., Utsunomiya, S., Reich, M., Kesler, S.E., Ewing, R.C., 2004, Invisible gold revealed: direct imaging of gold nanoparticles in a Carlin-type deposit: American Mineralogist, v. 89, p.1359–1366.

Putnis, A., 2002, Mineral replacement reactions: from macroscopic observations to microscopic mechanisms: Mineralogical Magazine, v. 66, p. 689–708.

Reich, M., Kesler, S.E., Utsunomiya, S., Palenik, C.S., Chryssoulis, S.L., Ewing, R.C., 2005, Solubility of gold in arsenian pyrite: Geochimica et Cosmochimca Acta, v. 69, p. 2781–2796.

Ribeiro, E.P.S., and Duarte, B.T., 2010, Projeto noroeste-nordeste de Mato Grosso folhas rio Guariba e rio Aripuanã escal 1:250.000: Goiânia, Serviço Geológico do Brasil- CPRM, 321p.

Richards, J.P., Wilkinson, D., and Ullrich, T., 2005, Geology of the Sari Gunay epithermal gold deposit, Nortwestern Iran: ECONOMIC GEOLOGY, v. 101, p.1455-1496.

Rodder, E., 1984., Fluid inclusions: Mineralogical Society of America, v.12, 646 p.

Rusk, B.G., Reed, M.H., and Dilles, J.H., 2008, Fluid inclusions evidence for magmatic-hydrothermal fluid evolution in the porphyry copper-molybdenum deposit at Bute, Montana: ECONOMIC GEOLOGY, v. 103, p.307-334.

Rye, R.O., 1993, The evolution of magmatic fluids in the epithermal environment; the stable isotope perspective: ECONOMIC GEOLOGY, v. 88, p. 733-752.

Santos, J.O.S., Hartmann, L.A., Gaudette, H.E., Groves, D.I., McNaughton, N.J., Fletcher, I.R. 2000, A new understanding of the Provinces of the Amazon Craton based on integration of field mapping an U-Pb and Sm-Nd geochronology. Gondwana Research, v. 3, p. 453-488.

Santos, J.O.S, Rizzoto, G.J., Potter, P.E., McNaughton, N.J., Matos, R.S., Hartmann, L.A., Chemale, Jr F., Quadro,s M.E.S. 2008,. Age and autochthonous evolution of the Sunsás Orogen in West Amazon Craton based on mapping and U–Pb geochronology: Precambrian Research, v. 165, p. 120-152.

Schmid-Beurmann, P., and Bente, K., 1995, Stability properties of CuS2–FeS2 solid solution series pyrite type: Mineral. Petrology, v.53, p. 333–341.

Seedorff, E., Dilles, J.H., Proffett, J.M., Jr., Einaudi, M.T., Zurcher, L. Stavast, W.J.A., Jhonson, D.A., and Barton, M.D., 2005, Porphyry deposits: Characteristics and origin of hypogene features: ECONOMIC GEOLOGY 100TH ANNIVERSARY VOLUME, p. 251-298.

Selby, D. and Creaser, R. A. 2003, Re–Os geochronology of organic-rich sediments: an evaluation of organic matter analysis methods: Chemical Geology, v. 200, p.225–240.

Sheppard, S.M.F., 1986, Characterization and isotopic variations in natural waters: Reviews in Mineralogy, v. 16, p. 165–183.

Shimazaki, H., and Clark, L. A., 1970, Synthetic FeS2–CuFe2 solid solution and fukuchilite-like minerals. Canadian Mineral. v.10, p. 648–664.

Shinohara, H., and Kazahaya, K., 1995, . (s.d.). Degassing processes related to magma chamber crystallization, in Thompson, J.F.H., Magmas, fluids, and ore deposits: Mineralogical Association of Canada Short Course Series, v. 23, p. 47–70.

Sillitoe, H.R., 2000, Gold-Rich Porphyry Deposits: Descriptive and genetical models and their role in the exploration and discovery: Society of Economic Geologist. SEG Reviews, v. 13, p. 315-345.

Silva, M.G., and Abram, M.B., 2008, Projeto metalogenia da Província Aurífera Juruena-Teles Pires, Mato Grosso Informe de Recursos Minerais, Programa Geologia do Brasil, CPRM-Serviço Geológico do Brasil, Série Ouro, no. 16, 212p. Goiânia. Serviço Geológico Brasileiro, CPRM, 212p.

Simon, G., Huang, H., Penner-Hahn, J.E., Kesper, S.E., Kao, L.S., 1999, Oxidation state of gold and arsenic in gold-bearing arsenian pyrite: American Mineralogist, v.84, p.1071–1079.

Smoliar, M. I., Walker, R. J. and Morgan, J. W., 1996, Re–Os ages of Group IIA, IIIA, IVA, and IVB iron meteorites: Science, v. 271, p. 1099–1102.

Souza, J.P., Frasca, A.A.S., Oliveira, C.C. 2005, Província Mineral de Alta Floresta. Relatório Integrado. Serviço Geológico Brasileiro, CPRM, Brasília, 164p.

Sterner, S.M., Hall, D.L., and Bodnar, R.J., 1988, Synthetic fluid inclusions. V. Solubility relations in the system NaCl-KCl-H_2O under vapor-saturated conditions: Geochimca *et* Cosmochimica Acta, v. 48, p. 989-1005.

Tang K.F., Li, J.W, Selby, D., Zhou, M.F., Bi, S.J., and Deng, X.D., 2013, Geology, mineralization, and geochronology of the Qianhe gold deposit, Xiong'ershan area, southern North China Craton: Mineralium Deposita, v. 48, p.729-747.

Taylor, H.P., 1979, Oxygen and hydrogen isotope relationships in hydrothermal mineral deposits, *in* Barnes, H.L., ed., Geochemistry of hydrothermal ore deposits, 2nd ed.: New York, Jhon Wiley & Sons, p.236-2777.

Thompson, J.F.H., Sillitoe, R.H., Baker, T., Lang, J.R., and Mortensen,J.K., 1999, Intrusion-related gold deposits associated with tungsten-tin provinces: Mineralium Deposita, v. 34, p. 323–334.

Ulrich, T., Günther, D., and Heinrich, C.A., 2002, The evolution of a porphyry Cu-Au deposit, based on LA-ICP-MS analysis of fluid inclusions: Bajo de la Alumbrera, Argentina: ECONOMIC GEOLOGY, v. 97, p. 1743-1774.

Williams, I.S, U-Th-Pb geochronology by ion microprobe, in McKibben, M.A., Shanks III, W.C., Ridley, W.I., 1998. (s.d.). Applications of Microanalytical Techniques to Understanding Mineralizing Processes: Reviews in Economic Geology, v.7, p. 1–35.

Wilson, A.J., Cooke, D.R., Harper, B,J., and Deyell, C.L., 2007, Sulfur isotopic zonation in the Cadia district, southeastern Australia: exploration significance and implications for the genesis of alkalic porphyry gold–copper deposits: Mineralium Deposita, v.42, p. 465-487.

Xavier, R. P., Assis, R. R., Creaser, R., Trevisan, G. V., Paes de Barros, A.J, Acevedo, A., Miguel-Junior, E., Barros, M. S. A., and Pinho, F. E. C, 2013. Timing of gold metallogeny in the Alta Floresta Gold Province: Evidence from pyrite and molybdenite Re-Os isotopic dating: 13 Congresso Geologia da Amazônia, Belém (PA), Brazil, 4p.

Yang, Y. F., Li, N., and C, Y.J., 2012, Fluid inclusion study of the Nannihhu giant porphyry Mo-W deposit, Henan province, China: Implications for the nature of porphyry ore-fluid system formed in continental collision setting: Ore Geology Reviews, v.46, p.83-94.

Zhang, J., Ye, H.S, Zhou, K., and Meng. F., 2014, Processes of ore genesis at the world-class Yuchiling molybdenum deposit, Henan province, China: Journal os Asian Earth Sciences, v. 79, p. 66-681.